Comparative study of novel maturation pathway in iPSC-derived cardiomyocytes via FOXO1/FOXM1 reveals improved maturation strategies

By Farid Elcure Alvarez

MSc Cancer, Stem Cells, and Developmental Biology
Minor Research Profile
Student Number: 5666880
Utrecht University

Supervised by Prof. Richard T. Lee and Dr. Nivedhitha Velayutham
Harvard Stem Cell Institute

Examined by Prof. Dr. Joost Sluijter
University Medical Center Utrecht

17th June 2023

Utrecht University

HARVARD UNIVERSITY

Abstract

Ischemic heart disease affects a significant part of the world's population. Induced pluripotent stem cell-cardiomyocyte (iPSC-CM) transplantation strategies are attractive treatments for ischemic heart disease due to their repair of endogenous cardiac function. However, cardiac remuscularization strategies are still under development due to side effects that lead to life-threatening arrhythmias associated with an immature iPSC-CM phenotype. Here, we improved iPSC-CM maturation in vitro by mimicking postnatal signaling switches to overcome arrhythmias after iPSC-CM transplantation. We compared different soluble factor-based treatments in 3D cell culture to improve current iPSC-CM maturation protocols by characterizing key parameters of CM maturation. Such parameters included mRNA and protein expression of sarcomere and ion channel genes measured via qPCR and flow cytometry, oxygen consumption rate via Seahorse XF cell mito stress test, and contractility via multielectrode array. We showed iPSC-CM in prolonged 3D cultures are still responsive to FOXO1/FOXM1 alterations, suggesting a new way to improve iPSC-CM maturation in vitro in combination with 3D and prolonged culture. Our ion channel expression and multielectrode array data showed relevant iPSC-CM maturation after P53 activation and FOXM1 inhibition when compared to other treatments. We also found both P53 activation and FOXO1 activation are comparable in inducing metabolic maturation in iPSC-CM. Lastly, combining P53 activation with other maturation methods, like mTOR inhibition, offered improved maturation in 3D, representing a new iPSC-CM maturation strategy. Thus, we concluded FOXO1 activation/FOXM1 inhibition is a novel iPSC-CM maturation pathway, although the P53 pathway is more beneficial to iPSC-CM maturation in comparison to other pathways.

Layman's Summary

Ischemic heart disease is a disease that causes reduced blood flow to your heart and affects approximately 126 million people worldwide. Researchers are exploring the use of induced pluripotent stem cells (iPSCs) to treat this disease by transplanting lab-grown heart cells made from iPSCs. The way this works is that iPSCs are adult cells (from your skin or blood for example) that are reprogrammed in the lab to become any cell in the human body, like a heart cell. However, one challenge is that these transplanted heart cells often cause dangerous heart rhythm problems. Researchers think this happens because the transplanted cells are immature, meaning they are more like the heart cells of a fetus than an adult. In this study, we improved the process of making heart cells from iPSCs so they would be more like the heart cells found in adults and avoid problems after their transplantation.

To achieve this, we tested different methods of making heart cells from iPSCs based on different aspects of cell communication and cell culture techniques. Specifically, we altered the function of four different cell communication proteins: FOXO1, FOXM1, mTOR, and P53, by either activating or blocking the protein function. All four of these proteins have a function during heart development. However, FOXO1 and FOXM1 have not been used to make heart cells from iPSCs yet. We compared all methods using three indicators of mature heart cells in an adult: the expression of specific genes and proteins, the cells' energy consumption, and their ability to beat.

We developed a new method of making heart cells from iPSCs by activating FOXO1 function and blocking FOXM1 function. In addition, we compared individual methods of making heart cells from iPSCs based on altering the function of four proteins: FOXO1, FOXM1, mTOR, and P53. We analyzed three indicators of mature (adult-like) heart cells and each of these methods offered different benefits in comparison to each other. Here, we also found that activating P53 function along with blocking mTOR function, resulted in more mature (adult-like) heart cells from iPSCs.

In conclusion, we identified a new way of making mature heart cells from iPSCs by altering the function of proteins FOXO1 and FOXM1. We also found that activating P53 function while blocking mTOR function is particularly beneficial for this maturation process compared to other methods. Our study shows new ways to prevent heart rhythm problems when treating ischemic heart disease with iPSC therapies.

Introduction

iPSC-CM promises clinical applications despite secondary complications.

Ischemic heart disease (IHD) is very widespread, affecting 126 million (1.72%) people worldwide [1]. Cardiomyocyte transplantation strategies are attractive treatments for ischemic heart disease due to their repair of endogenous cardiac function (Figure 1A). Moreover, transplantation of induced pluripotent stem cell (iPSC)-derived cardiomyocytes (CM) (iPSC-CM) for remuscularization therapies overcomes the limited availability of cardiac tissue donors. For example, the transplantation of human embryonic stem cell-derived CM or iPSC-CM re-muscularized infarcted non-human primate hearts [2,3], infarcted pig hearts [4], and infarcted rat hearts [5]. However, cardiac remuscularization strategies are still under development due to side effects that lead to life-threatening arrhythmias in large animal models [2–4].

Arrhythmias peaked at 10 days post-transplant and decreased over time in pig hearts (Figure 1B) [4]. Coinciding with the decrease in arrhythmias over time, graft maturation was observed over time in non-human primate hearts [3]. Here, human embryonic stem cell-derived CM showed maturation by displaying characteristics of adult tissue cardiomyocytes, such as similar myofibril alignment, sarcomere registration, and CM diameter [3]. Therefore, arrhythmias after transplantation are associated with immature stem cell-derived CM that do not resemble tissue CM, meaning iPSC-CM maturation is key for preventing arrhythmias.

Signaling switches in postnatal cardiomyocytes are key for inducing iPSC-CM maturation.

Current iPSC-CM maturation strategies are based on molecular switches from fetal to postnatal cardiomyocyte that reflect phenotype changes (Figure 1C) [6,7]. For example, these phenotype changes include changes in cell cycle progression, metabolism, and electrical maturation because of postnatal switches (Figure 1D). Common iPSC-CM maturation treatments with fatty acids, thyroid and glucocorticoid hormones, and three-dimensional (3D) or prolonged culture induce similar phenotype changes that resemble signaling switches in cardiac development (Figure 1D) [8–12]. As such, signaling switches in postnatal CM are key for inducing CM maturation.

Metabolic signaling pathways in postnatal CM development are targeted to develop iPSC-CM maturation treatments based on biochemical soluble factors in recent years. Nutrient signaling pathways that overlap with quiescence signaling, like the mammalian target of rapamycin (mTOR) pathway, have shown increased iPSC-CM maturation in 2D culture (Figure 2A) [13]. iPSC-CM maturation is measured in multiple ways, such as changes towards oxidative respiration [14], increased contractility and ion channel expression [15], and switches in sarcomere isoform expression [16–18]. Here, mTOR inhibition via the soluble factor Torin-1 increased mRNA expression of mature ion channels as a measure of electrophysiological maturation [13]. Similarly, mTOR inhibition increased the oxygen consumption rate, signifying a metabolic maturation switch [13].

Likewise, other measures such as increased sarcomere protein expression, increased relative maximum systolic force, and induction of quiescence after mTOR inhibition indicated iPSC-CM maturation [13].

Furthermore, mTOR inhibition via Torin-1 resulted in increased p53 protein expression (Figure 2A) [13]. Soluble factor Nutlin3a, which upregulates p53, achieved similar iPSC-CM maturation in comparison to Torin-1 mTOR inhibition [13]. Therefore, Garbern's data showed p53 upregulation drives iPSC-CM maturation in the mTOR pathway. Yet, further molecular mechanisms remained unexplored from the mTOR-p53 pathway in iPSC-CM maturation.

Optimize iPSC-CM maturation for improved electrical maturation.

Interestingly, p53 activation via Nutlin3a led to changes in forkhead box protein (FOX) factor expression involved in CM maturation, as shown by mRNA expression analysis after maturation treatment (Figure 2B, C). We hypothesized Forkhead box (FOX) protein O1 (FOXO1)/ FOX protein M1 (FOXM1) participate in iPSC-CM maturation downstream of the p53 activation pathway since other studies have shown the role of FOXO1/FOXM1 regulation in neonatal CM quiescence [19]. Here, FOXM1 is expressed in fetal CM and promotes cell cycle progression (Sengupta et al., 2012). Contrastingly, FOX O factors like FOXO1 and FOX protein O3 (FOXO3) are expressed in post-natal CM, where they translocate to the nucleus to inhibit FOXM1 and promote cell cycle withdrawal [19].

To evaluate FOXO1/FOXM1 involvement in iPSC-CM maturation, the Richard T. Lee lab used soluble factors to alter FOXO1 and FOXM1 activity (Figure 2B). FOXO1 activator LOM612 or FOXM1 inhibition RCM-1 treatment increased higher ion channel expression in iPSC-CM, inducing a more mature phenotype (Figure 3E). Moreover, single-cell RNA sequencing done by the Richard T. Lee lab confirmed the association between p53 activation and FOXO1/FOXM1 (data not shown). Furthermore, cell cycle and electrophysiological characterization done by the Lee lab supported the iPSC-CM maturation effect of the FOXO1 activation or FOXM1 inhibition treatment (data not shown). These results indicated that FOXO1 activation and FOXM1 inhibition have similar effects as the p53 activation pathway during the iPSC-CM maturation. Therefore, FOXO1 activation and FOXM1 inhibition likely function as downstream effectors of the mTOR-p53 iPSC-CM maturation pathway, although direct evidence is needed to confirm this hypothesis.

To overcome arrhythmias after iPSC-CM transplantation we aimed to improve iPSC-CM maturation in vitro. We studied a direct comparison between soluble factor-based treatments while further adding the 3D culture technology to improve current iPSC-CM maturation protocols. Our main goal was to improve electrophysiological iPSC-CM maturation by inducing postnatal signaling switches. Here, we tackled our aim by characterizing key parameters of CM maturation while defining the advantages of individual soluble factor treatments for iPSC-CM maturation.

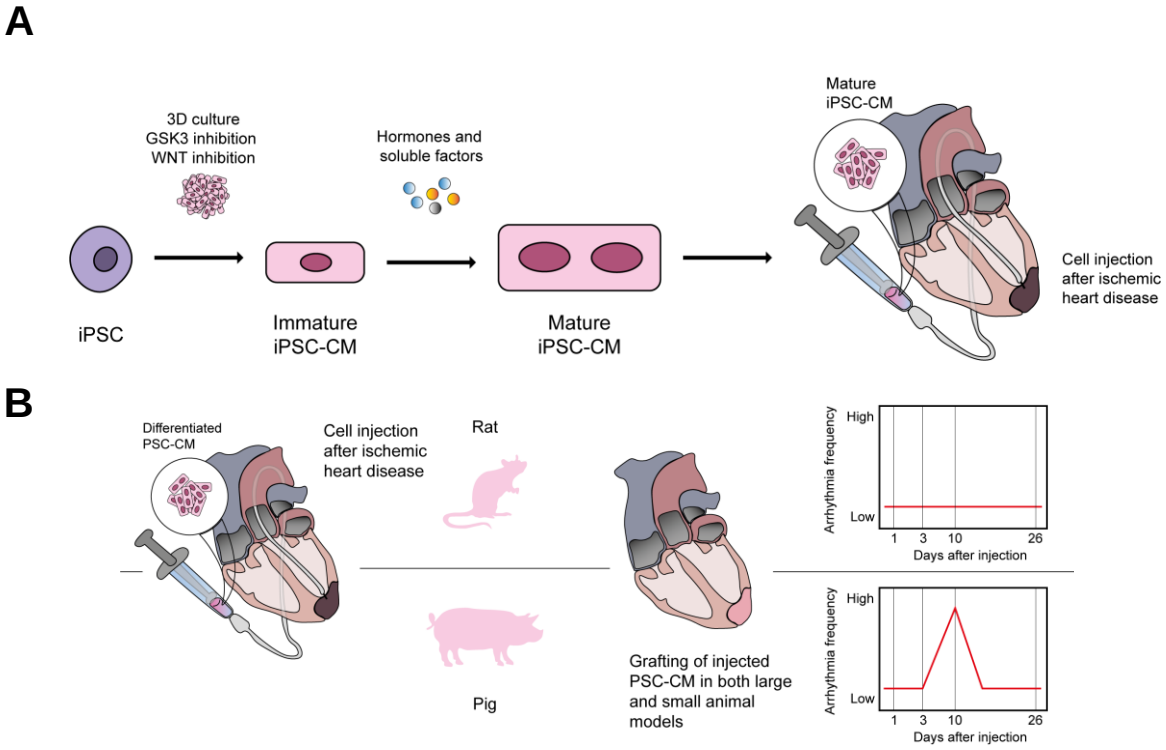
A
3D culture
GSK3 inhibition
WNT inhibition
Hormones and
soluble factors
Mature
iPSC-CM
iPSC
Immature
iPSC-CM
Mature
iPSC-CM
Cell injection
after ischemic
heart disease
B
Differentiated
PSC-CM
Cell injection
after ischemic
heart disease
Rat
Pig
Grafting of injected
PSC-CM in both large
and small animal
models
Arrhythmia frequency
High
Low
1
3
10
26
Days after injection
C
Cardiac Proliferation
Cardiac Hypertrophy, Cell Cycle Exit
Hippo
Normoxia
Meis
NOTCH
WNT
HIF1
T3
Insulin
IGF1
VEGF
mTOR
Pi3K
AKT
AMPK
Birth
Embryonic Cardiomyocyte
Postnatal Cardiomyocyte
D
iPSC
Immature
iPSC-CM
Altered cellular
energy sources
Prolonged culture
Hormones and
soluble factors
Biophysical
stimulation
3D culture
Co-culture
Mature
iPSC-CM
Cell cycle exit
Sarcomere
isoform switching
Oxidative
phosphorylation
Contractility
Ion channel
expression

Figure 1. Illustration of current applications and limitations of iPSC-CM transplantation for cardiac revascularization after ischemic heart disease. A) Schematic representation of iPSC-CM differentiation and clinical applications for cardiac revascularization after ischemic heart disease [20–22]. (B) Schematic representation of secondary complications arising from an immature phenotype after iPSC-CM transplantation following ischemic heart disease [2–4]. C) Adapted illustration of pathways involved in cardiomyocyte maturation after birth [7]. (D) Illustration of iPSC-CM maturation methods and readouts. [8–10,23,24].

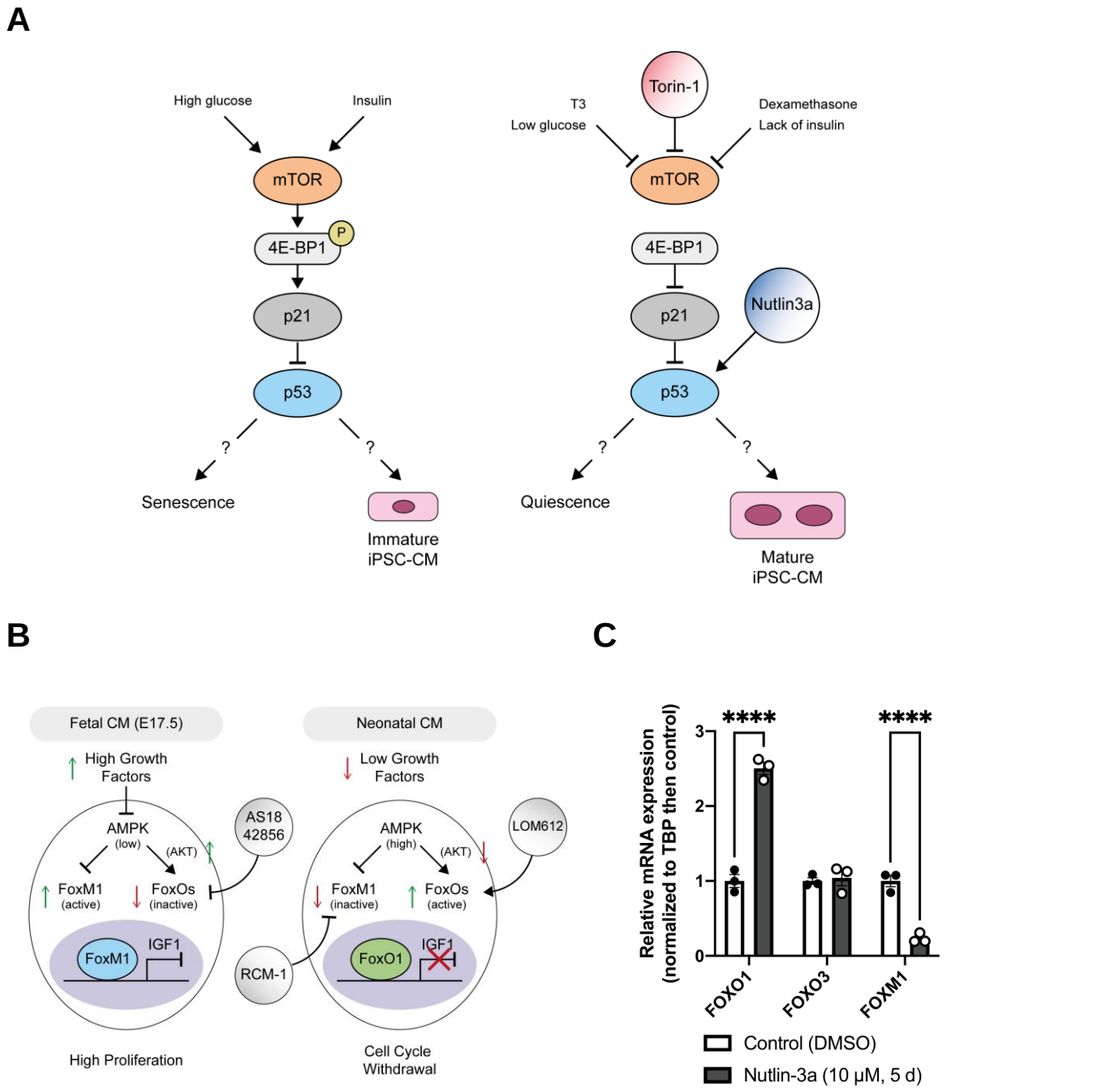

Figure 2. Illustration of soluble factor-based maturation methods for iPSC-CM. (A) Adapted illustration of mTOR inhibition and P53 activation pathway in iPSC-CM maturation [13]. (B) Adapted illustration of FOXM1 inhibition and FOXO1 activation pathway inducing cell cycle withdrawal in CM development [19]. (C) Relative mRNA expression of FOXO1, FOXO3, and FOXM1 by qPCR after Nutlin3a treatment starting at day 9 of iPSC-CM differentiation, normalized to TBP, and then to control DMSO treatment (unpublished data from Richard T. Lee Lab). ****p<0,0001 by two-way ANOVA with Dunnett's multiple comparison test compared to the control treatment (n=3 samples per condition).

Materials and Methods

iPSC 2D culture and iPSC-CM differentiation

The human iPSC line UCSD142i-86-1 (female donor, fibroblast-derived) was used in this study. This line was established by Dr. Kelly Frazer's laboratory at the University of California San Diego and was distributed by WiCell. iPSCs were maintained in StemFlex Medium (Thermo Fisher Scientific) and passaged every 3-4 days onto two-dimensional plates until passage 45. StemFlex Medium was refreshed every 1-2 days and supplemented with ROCK inhibitor Y27632 2HCl (5 µM, S1049, Selleck Chemicals) for 1 day after each passage. In addition, plates for iPSC culture were coated with Geltrex (1:100, Thermo Fisher Scientific) diluted in DMEM/F12 medium (Thermo Fisher Scientific) before each passage.

iPSC-CM differentiation

iPSCs on 2D plates were seeded into suspension culture 4 days before differentiation. Here, $4x10^6$ to $8x10^6$ cells were seeded in StemScale PSC Suspension Medium (Thermo Fisher Scientific) supplemented with ROCK inhibitor Y27632 2HCl (5 µM). The media volume used for iPSC-CM differentiation in 125 mL flasks was 20 mL unless otherwise specified. 3 days before differentiation, media was replaced with StemScale PSC Suspension Medium without ROCK inhibitor Y27632 2HCl supplementation. 3 days later, on day 0 of differentiation, RBA medium was prepared with RPMI 1640 medium (Thermo Fisher Scientific), supplemented with B-27™ Supplement minus insulin (2%, Thermo Scientific), and L-Ascorbic acid 2-phosphate sesquimagnesium salt hydrate (50 µg/mL, Sigma-Aldrich). On day 0, StemScale PSC Suspension Medium was replaced with RBI medium supplemented with GSK3 inhibitor CHIR-99021 (6 µM, Selleck Chemicals). After 24 hours, on day 1, the media was replaced with RBA medium. On day 2, 48 hours after, the medium was replaced with RBA supplemented with Stemolecule Wnt Inhibitor IWP-4 (6 µM, Reprocell). On day 4, the media was replaced with RBA medium. On day 7, RBI medium was prepared by supplementing RPMI 1640 medium with B-27™ Supplement minus insulin (2%), and Insulin solution human (10 µg/mL, Sigma-Aldrich). Afterward, the media was replaced with RBI medium on day 7, and every 2 to 3 days hereafter.

iPSC-CM maturation treatment

$4x10^6$ to $8x10^6$ iPSC-CMs forming beating cardiac spheroids were transferred on day 9 of the differentiation protocol on 6-well suspension plates for maturation treatments. Treatment media was refreshed on day 9 and day 11 for each sample, for a 5-day-long treatment. On day 14 after differentiation, each sample media was replaced by RBI medium, and refreshed every 2-3 days hereafter. Samples were harvested within the next 4 days after treatment.

The maturation treatment media was based on RBI medium and supplemented with the following soluble factors as indicated: Vehicle DMSO (0.1%, ATCC), LOM612 (5 µM, HY-101035,

MedChem Express), Nutlin3a (10 µM, S1061, Selleck Chemicals), Torin-1 (200 nM, S2827, Selleck Chemicals), RCM-1 (1 µM, S6898, Selleck Chemicals), AS1842856 (1 µM, S8222, Selleck Chemicals), and AICAR (1 mM, S1802, Selleck Chemicals).

The same method was followed for maturation treatments starting on day 45 of the differentiation protocol, with a few exceptions. Treatment media was refreshed on day 45 and day 47 for each sample, for a 5-day-long treatment. On day 50 after differentiation, treatment media was replaced by RBI medium, and refreshed every 2-3 days hereafter until harvested.

Flow cytometry

Following the maturation treatment, approximately $1x10^6$ to $2x10^6$ single cells per sample were dissociated from beating cardiac spheroids in culture using the STEMdiff Cardiomyocyte Dissociation Kit (StemCell) and replated onto U-bottom 96-well plates. The unstained and single-stain controls were plated by mixing aliquots of all cell suspensions. The plated cells were washed with eBioscience Flow Cytometry Staining Buffer Set (Invitrogen) and incubated with the extracellular antibody diluted in eBioscience Flow Cytometry Staining Buffer for 30 minutes at 22°C. Samples were washed twice with eBioscience Flow Cytometry Staining Buffer. All samples were fixated using the eBioscience FOXP3/Transcription Factor Staining Buffer Set (Invitrogen) by preparing the fixation/permeabilization working solution and incubating the samples for 20 minutes at 22°C. Samples were washed once with the permeabilization buffer from eBioscience FOXP3/Transcription Factor Staining Buffer Set. Intracellular antibodies were diluted using the permeabilization buffer from eBioscience FOXP3/Transcription Factor Staining Buffer Set, and incubated on the samples for 30 minutes at 22°C. Following the intracellular antibody incubation, the samples were washed thrice with eBioscience Flow Cytometry Staining Buffer Set, resuspended in the eBioscience Flow Cytometry Staining Buffer Set, and strained through 5 mL polystyrene round-bottom tube with cell-strainer cap (Falcon) before data collection. Data were acquired using the BD FACSymphony A5 Flow Cytometer (660964, BD Biosciences). We used FCS Express 7 (De Novo Software) to calculate the geometric mean fluorescence intensity and percentages of the gated cells for each sample.

Extracellular antibodies consisted of Rabbit Anti-Kir2.1/KCNJ2 (extracellular)-FITC Antibody (1:50, APC-159-F, Alomone labs), x Human Connexin 43 Alexa Fluor [750] (1:100, FAB7737S-100UG, R&D systems), and x Human CD36 Alexa Fluor [594] (1:200, FAB19551T-100UG, R&D systems). Intracellular antibodies consisted of FOXM1 (A-11) PE (1:100, sc-271746, Santa Cruz Biotechnology), BV421 Mouse Anti-Cardiac Troponin T (1:200, 565618, BD Biosciences), FKHRL1/FOXO3 (D-12) Alexa Fluor 680 (1:100, sc-48348 AF680, Santa Cruz Biotechnology), FKHR/FOXO1 (C-9) Alexa Fluor 790 (1:100, sc-374427 AF790, Santa Cruz Biotechnology), Alexa Fluor 647 Mouse Anti-Cardiac Troponin I (1:100, 564409, BD Biosciences), and Rabbit anti-Glut4 [PE] (1:100, NBP1-49533PE, Novus Bio).

Seahorse XF cell mito stress test

After the maturation treatment, approximately $1x10^6$ to $2x10^6$ single cells per sample were dissociated from beating cardiac spheroids in culture using the STEMdiff Cardiomyocyte Dissociation Kit (StemCell) according to the manufacturer's instructions. Cells were plated in a Seahorse XF96 Cell Culture Microplate (Agilent) coated with Geltrex (1:100 in DMEM/F12, Thermo Fisher Scientific) at a 150.000 cell density per well. The medium was replaced with RBI medium 1 day after replating. 2 days after replating, the Seahorse XF Cell Mito Stress Test Kit (Agilent) was used to determine the oxygen consumption rate (OCR) and extracellular acidification rate (ECAR) of each sample according to the manufacturer's instructions. Samples were measured in the Seahorse XFe96 Analyzer (Agilent) and cell density per well was quantified using the CyQUANT Cell Proliferation Assay (Invitrogen) according to the manufacturer's instructions. OCR and ECAR data for each well were normalized to cell numbers obtained from the CyQUANT Cell Proliferation Assay using the Seahorse Wave Desktop Software (Agilent).

The following parameters were calculated per well based on the different time points of OCR measurements: basal respiration (baseline measurement 3 minus rotenone & antimycin A measurement 12), ATP-linked respiration (baseline measurement 3 minus oligomycin measurement 12), maximal respiratory capacity (FCCP measurement 8 minus rotenone & antimycin A measurement 12), respiratory reserve capacity (FCCP measurement 8 minus baseline measurement 3), and non-mitochondrial OCR (rotenone & antimycin A measurement 12).

mRNA Extraction, cDNA Synthesis, and qPCR

RNA was isolated from samples after the maturation treatment using the E.Z.N.A. Total RNA kit I (Omega) and following the manufacturer's instructions. In addition to the E.Z.N.A. Total RNA kit I, 2-Mercaptoethanol (Sigma), and the DNase I digestion set (Omega) were used as indicated in the kit. The High-capacity cDNA reverse transcription kit (Applied Biosystems) was used to synthesize cDNA from the RNA samples. Quantitative polymerase chain reaction (qPCR) was performed using the synthesized cDNA, the primer pairs listed below, the Bio-Rad iTaq Universal SYBR Green Mix (Bio-Rad), and the CFX384 Touch Real-Time PCR Detection System (Bio-Rad). The double delta Ct method was used to calculate the mRNA expression of each sample relative to the TATA-binding protein (TBP) housekeeping gene.

The following forward (F) and reverse (R) primer pairs were used: TBP2 F (CCCGAAACGCCGAATATAATCC), TBP2 R (AATCAGTGCCGTGGTTCGTG), TNNT2-1 F (GGAGGAGTCCAAACCAAAGCC), TNNT2-1 R (TCAAAGTCCACTCTCTCTCCATC), MYH6 F (GCCCTTTGACATTCGCACTG), MYH6 R (GGTTTCAGCAATGACCTTGCC), MYH7 F (TCACCAACAACCCCTACGATT), MYH7 R (CTCCTCAGCGTCATCAATGGA), TNNI3 F (TTTGACCTTCGAGGCAAGTTT), TNNI3 R (CCCGGTTTTCCTTCTCGGTG), ATP2A2 F (ATGGGGCTCCAACGAGTTAC), ATP2A2 R (TTTCCTGCCATACACCCACAA), CACNA1C F (TGATTCCAACGCCACCAATTC),

CACNA1C R (GAGGAGTCCATAGGCCATTACT), KCNJ2 F (TGGATGCTGGTTATCTTCTGC), KCNJ2 R (AGCCTATGGTTGTCTGGGTCT), SCN5A F (TCTCTATGGCAATCCACCCCA), SCN5A R (GAGGACATACAAGGCGTTGGT), TNNI1 F (CCGGAAGTCGAGAGAAAACCC), TNNI1 R (TCAATGTCGTATCGCTCCTCA), GLUT4 F (GCTCATCCTTGGACGATTCC), GLUT4 R (CACCTGGGCGATCAGAATG), PPARGC1A F (TCTGAGTCTGTATGGAGTGACAT), PPARGC1A R (CCAAGTCGTTCACATCTAGTTCA), TP53 F (CAGCACATGACGGAGGTTGT), TP53 R (TCATCCAAATACTCCACACGC), FOXO1 F (TCGTCATAATCTGTCCCTACACA), FOXO1 R (CGGCTTCGGCTCTTAGCAAA), FOXO1 R (CGGCTTCGGCTCTTAGCAAA), FOXO3 F (CGGACAAACGGCTCACTCT), FOXO3 R (GGACCCGCATGAATCGACTAT), FOXM1 F (CGTCGGCCACTGATTCTCAAA), FOXM1 R (GGCAGGGGATCTCTTAGGTTC).

Multielectrode array

Beating cardiac spheroids from each sample were dissociated into single cells using the STEMdiff Cardiomyocyte Dissociation Kit (StemCell) after the maturation treatment. For each sample replicate, 250000 cells were seeded per well in an 8 µL droplet. These cells were seeded onto a Geltrex-coated CytoView MEA 24-well plate (Axion Biosystems). Following a 1-hour incubation at 37°C, the medium was carefully added to each well following STEMdiff Cardiomyocyte Dissociation Kit instructions. After cell seeding, RBI medium was refreshed every 2-3 days until the cells were measured. Approximately 4 to 6 days after cell seeding, the CytoView MEA 24-well plates were measured on the Maestro Edge multiwell microelectrode array (MEA) and Impedance system (Axion Biosystems). The beat amplitude of sample cardiomyocytes was determined via unpaced cardiac field potential and cardiac contractility readings from the Cardiac Module analysis tool (Axion Biosystems).

Data analysis

Statistical analyses and data plotting were performed using GraphPad Prism 9 software (Dotmatics). Data were reported as mean ± standard error of the mean (SEM) and analyzed with Brown-Forsythe and Welch ANOVA with Dunnett's T3 multiple comparison test, with individual variances computed for each comparison. Figure legends include exact statistical tests used, values of n, and significance thresholds used. Tests were considered statistically significant for $p<0.05$.

Results

The effects of FOXO1/FOXM1 manipulation are enhanced at later time points of differentiation.

Initially, we decided to combine soluble factor maturation treatments with 3D culture and prolonged culture, which are consolidated methods to generate more mature tissue-like iPSC-CM [12,23]. We treated cells with the soluble factors LOM612 (FOXO1 activation), AS1842856 (FOXO1 inhibition), and RCM-1 (FOXM1 inhibition) starting at 9 or 45 days after differentiation to evaluate phenotypical changes in maturation (Figure 3A). We used beating iPSC-CM 3D suspension cultures and analyzed the protein expression of sarcomere and ion channel genes for both time points of the maturation treatment. Moreover, we examined metabolic changes in oxidative phosphorylation for both time points of the maturation treatment.

We examined the protein expression of cardiac troponin T2 (TNNT2), the inward-rectifier potassium channel Kir2.1 (Kir2.1 also known as KCNJ2), FOXO1, FOXO3, and FOXM1 via flow cytometry (Figure 3B-G, S1). TNNT2 is a key sarcomere structural protein that is fundamental for the contractile apparatus of post-natal cardiomyocytes and is upregulates in iPSC-CM differentiation and maturation [24,25]. KCNJ2 is an important establisher of the potassium current that results in cardiomyocyte hyperpolarization and low resting membrane potential, key for electrical maturation of postnatal CM [26,27].

FOXO1 activation via LOM612 and FOXM1 inhibition via RCM-1 led to increased TNNT2 protein expression starting at day 9 of differentiation (Figure 3C). In contrast, FOXO1 inhibition via AS1842856 starting at day 9 of differentiation led to a significant decrease in the TNNT2 expression (Figure 3B-C). In a similar trend, FOXM1 inhibition via RCM-1 increased the percentage of KCNJ2-positive cells after 9 days of differentiation, whereas FOXO1 activation via LOM612 and FOXO1 inhibition via AS1842856 significantly increased the mean fluorescence intensity of KCNJ2. Interestingly, we observed a drastic increase in KCNJ2 expression after FOXM1 inhibition via RCM-1 starting at 45 days of differentiation (Figure 3G). Similarly, after AS1842856 FOXO1 inhibition starting at 45 days of differentiation, the decrease in TNNT2 expression was further accentuated (Figure 3D). Therefore, the prolonged culture accentuated the effects of RCM-1 and AS1842856, indicating iPSC-CM maturation can be further improved in prolonged cultures via FOXM1 inhibition.

In addition to protein expression, we determined metabolic changes via the seahorse XF cell mito stress test and measured the oxygen consumption rate at different time points (Figure 4, S2A-B). The Seahorse XF Cell Mito Stress Test uses electron transport chain modulators at different time points to determine metabolic parameters based on oxygen consumption rate (OCR). Here, we used carbonyl cyanide-4 (trifluoromethoxy) phenylhydrazone (FCCP), oligomycin, rotenone, and antimycin A as the electron transport chain inhibitors to calculate key parameters of mitochondrial

function. We expected a statistically significant increase in basal respiration, maximum respiration, and ATP-linked respiration in mature iPSC-CM [28].

We observed metabolic changes in the OCR profile in FOXO1 activation and FOXO1 inhibition starting after 9 days of differentiation, while FOXM1 inhibition resembled the OCR profile of the control (Figure 4A, D, G). FOXO1 activation via LOM612 caused an increase in maximal respiration after the FCCP injection, while FOXO1 inhibition via AS1842856 achieved the same effect. Furthermore, basal respiration increased after FOXO1 activation via LOM612 at 9 days of differentiation (Figure 4A). We observed similar trends after maturation treatments starting at day 45 of differentiation (Figure 4B-C, E-F, H-I). Here, FOXO1 activation via LOM612 significantly increased basal respiration in prolonged cultures, while all other parameters were increased non-significantly (Figure 4B-C). Unlike the treatments starting at day 9, FOXO1 inhibition via AS1842856 increased OCR parameters non-significantly at 45 days of differentiation. This indicated iPSC-CM matured in prolonged culture were less sensitive to metabolic changes induced by FOXO1 inhibition. Lastly, day 45 treatment of FOXM1 inhibition via RCM-1 had comparable OCR parameters to the control, except for a decrease in ATP-linked respiration.

Together, our results indicated that iPSC-CM in prolonged culture were still sensitive to FOXO1/FOXM1 alterations. The effects of FOXM1 inhibition increasing KCNJ2 expression and FOXO1 activation increasing OCR parameters were further accentuated after prolonged culture of iPSC-CM. Therefore, when logistically feasible, we demonstrated combining soluble factor treatments and prolonged cultures is beneficial for applications in iPSC-CM maturation in comparison to short-term methods.

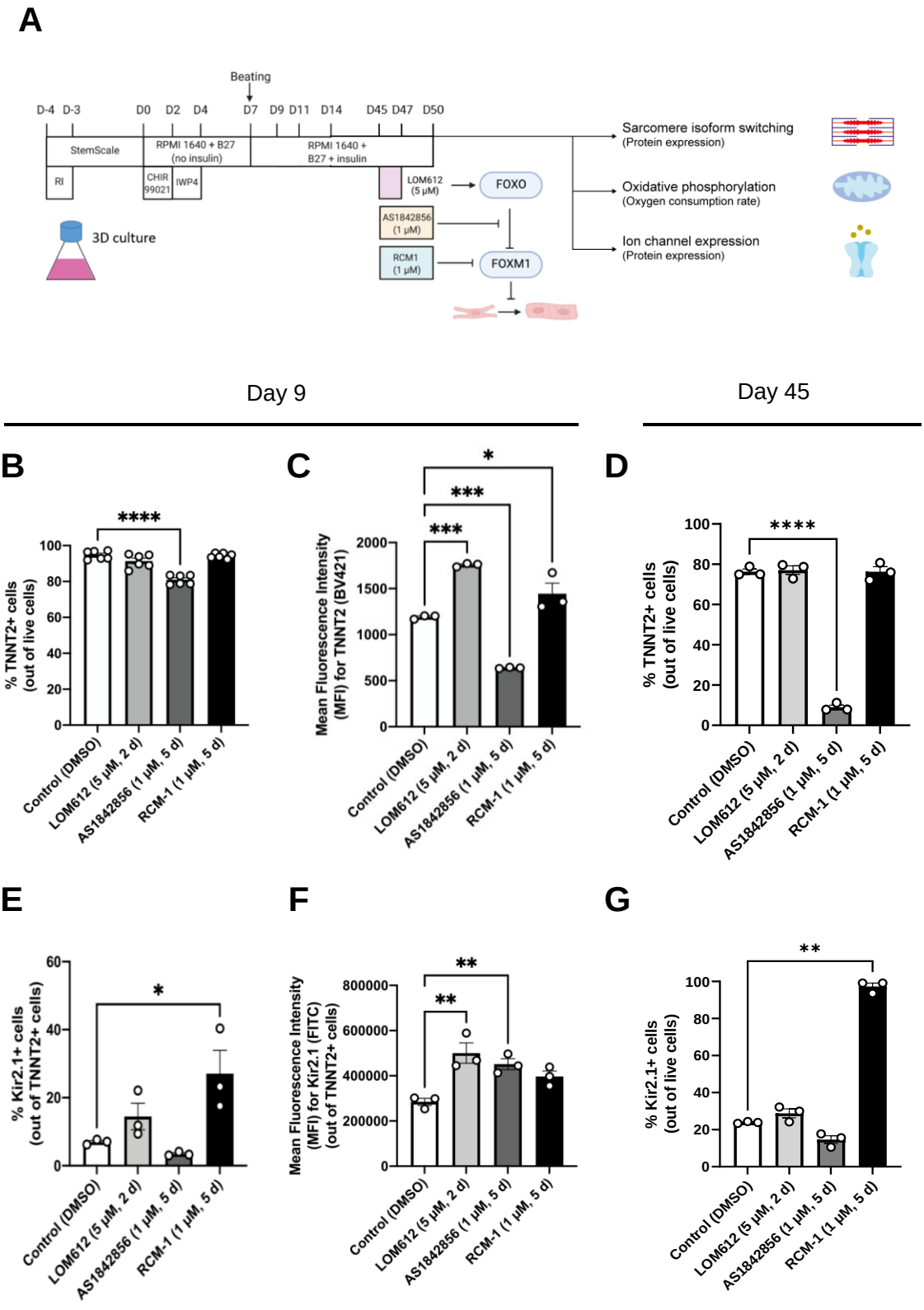
A
Beating
D-4 D-3
D0 D2 D4
D7 D9 D11 D14
D45 D47 D50
StemScale
RPMI 1640 + B27 (no insulin)
RPMI 1640 + B27 + insulin
RI
CHIR 99021
IWP4
LOM612 (5 μM)
FOXO
AS1842856 (1 μM)
RCM1 (1 μM)
FOXM1
3D culture
Sarcomere isoform switching (Protein expression)
Oxidative phosphorylation (Oxygen consumption rate)
Ion channel expression (Protein expression)
Day 9
Day 45
B
% TNNT2+ cells (out of live cells)
C
Mean Fluorescence Intensity (MFI) for TNNT2 (BV421)
D
% TNNT2+ cells (out of live cells)
E
% Kir2.1+ cells (out of TNNT2+ cells)
F
Mean Fluorescence Intensity (MFI) for Kir2.1 (FITC) (out of TNNT2+ cells)
G
% Kir2.1+ cells (out of live cells)
Control (DMSO)
LOM612 (5 μM, 2 d)
AS1842856 (1 μM, 5 d)
RCM-1 (1 μM, 5 d)

Figure 3. FOXO1/FOXM1 alterations via soluble factors have enhanced maturation effects in day 45 treated iPSC-CM. (A) Schematic representation of soluble factor maturation treatment in 3D long-term cultures analyzed by protein expression via FACS, and oxygen consumption rate via seahorse XF cell mito stress test. (B) Percentage of TNNT2 expressing cells after soluble factor treatments starting at day 9 of differentiation treatment (unpublished data from Richard T. Lee Lab) (D) and at day 45 of differentiation by flow cytometry. (C) Mean fluorescence intensity of TNNT2-BV421 staining after soluble factor treatments starting at day 9 of differentiation by flow cytometry treatment (unpublished data from Richard T. Lee Lab). (E) Percentage of Kir2.1 expressing cells after soluble factor treatments starting at day 9 of differentiation treatment (unpublished data from Richard T. Lee Lab) (G) and at day 45 of differentiation by flow cytometry. (F) Mean fluorescence intensity of Kir2.1-FITC staining after soluble factor treatments starting at day 45 of differentiation by flow cytometry treatment (unpublished data from Richard T. Lee Lab). *p<0.05, **p<0.005, ***p<0,0005, ****p<0,0001 by one-way ANOVA with Brown-Forsythe and Welch multiple comparison analysis compared to the control treatment (n=3 samples per condition, plotted as mean +/- SEM).

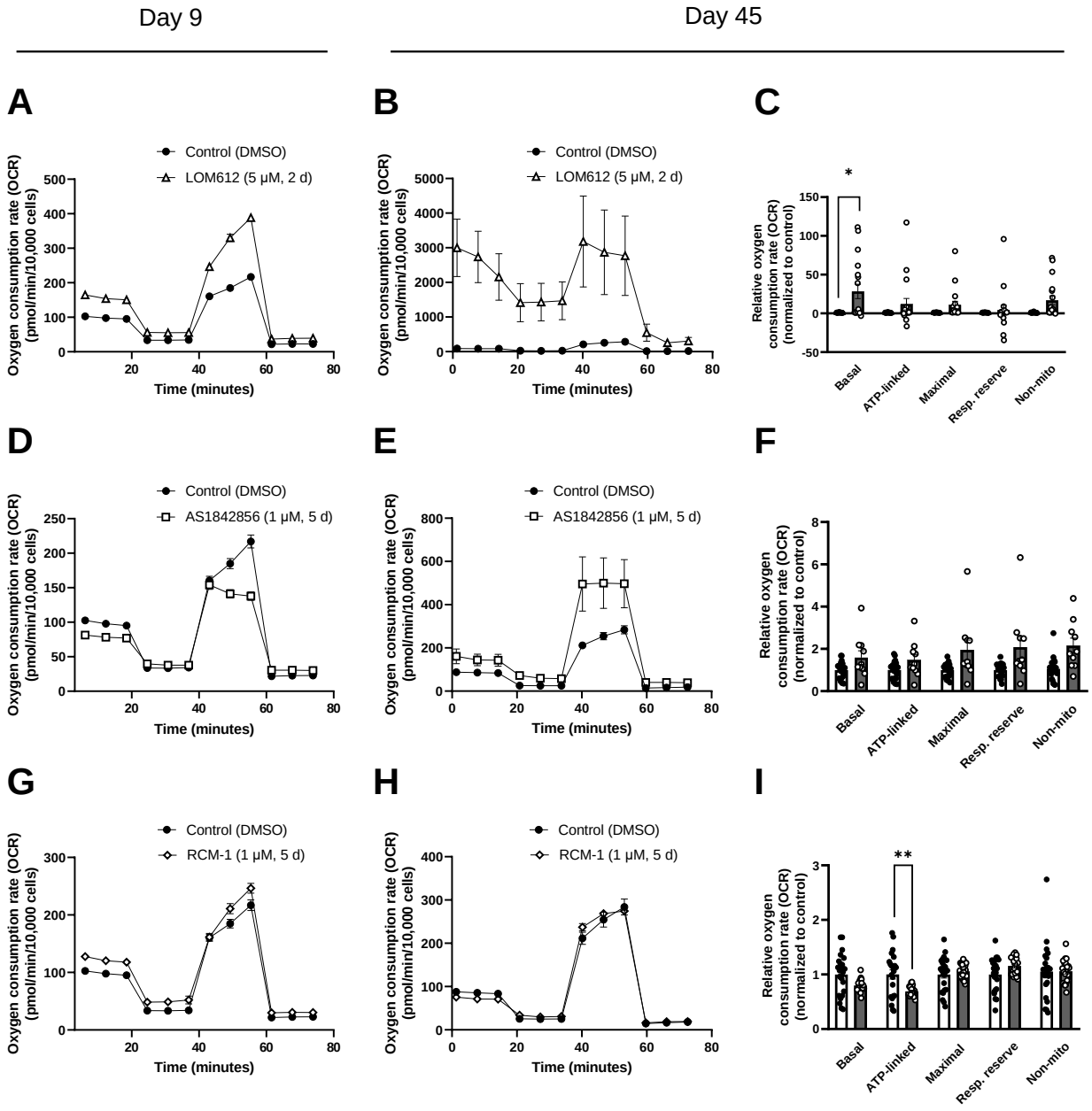
Day 9
Day 45
A
B
C
Control (DMSO)
LOM612 (5 μM, 2 d)
Oxygen consumption rate (OCR) (pmol/min/10,000 cells)
Time (minutes)
Relative oxygen consumption rate (OCR) (normalized to control)
Basal
ATP-linked
Maximal
Resp. reserve
Non-mito
D
E
F
AS1842856 (1 μM, 5 d)
G
H
I
RCM-1 (1 μM, 5 d)

Figure 4. FOXO1/FOXM1 soluble factor treatment induces similar maturation effects on day 45 treated iPSC-CM. (A) Oxygen consumption rate profile after LOM612 treatment starting at day 9 of differentiation (B) and day 45 of differentiation measured by Seahorse XF cell mito stress test. (C) Oxygen consumption rate parameters after LOM612 starting at day 45 of differentiation relative to control DMSO treatment. (D) Oxygen consumption rate profile after AS1842856 treatments starting at day 9 of differentiation (E) and at day 45 of differentiation measured by Seahorse XF cell mito stress test. (F) Oxygen consumption rate parameters after AS1842856 starting at day 45 of differentiation relative to control DMSO treatment. (G) Oxygen consumption rate profile after RCM-1 treatments starting at day 9 of differentiation (H) and at day 45 of differentiation measured by Seahorse XF cell mito stress test. (I) Oxygen consumption rate parameters after RCM-1 starting at day 45 of differentiation relative to control DMSO treatment. *$p<0.05$, **$p<0.005$ by one-way ANOVA with Brown-Forsythe and Welch multiple comparison analysis compared to the control treatment (DMSO n=23 wells from 3 samples, LOM612 n=18 wells from 3 samples, AS1842856 n=10 wells from 3 samples, RCM-1 n=21 wells from 3 samples, plotted as mean +/- SEM).

P53 activation and FOXM1 inhibition show the most significant changes in cardiac muscle and ion channel expression in iPSC-CM at D9

After studying the effects of FOXO1 activation and FOXM1 inhibition in prolonged iPSC-CM maturation, we evaluated how maturation by FOXO1/FOXM1 alterations compared to other established soluble factor methods. We compared the FOXO1/FOXM1 alterations with p53 activation via Nutlin3a, and mTOR inhibition via Torin-1 (Figure 5A). Furthermore, we combined our soluble factor treatments with 3D culture after which we examined protein and mRNA expression via flow cytometry and qPCR respectively, and contractility changes via multielectrode array (Figure 5, S4).

In our protein expression analysis, TNNT2 expression significantly increased after p53 activation via Nutlin3a treatment in comparison to other soluble factor treatments (Figure 5B, S4A). On the other hand, FOXO1 inhibition via AS1842856 drastically decreased TNNT2 expression (Figure 5B). Additionally, Nutlin3a increased FOXO1 and FOXO3 protein expression in comparison to all treatments, while complementarily decreasing the number of FOXM1-positive cells (Figure S4C-H). Moreover, protein expression of KCNJ2 greatly increased after RCM-1, and Nutlin3a treatment (Figure 5D).

We also measured mRNA expression of TNNT2, TNNI3, myosin heavy chain 6 (MYH6), and myosin heavy chain 7 (MYH7) to study sarcomere maturation (Figure 5C). MYH6 to MYH7 isoform switching is characteristic of CM maturation in humans, where post-natal CM expresses higher MYH7 than MYH6 [29]. Despite Nutlin3a treatment increasing TNNT2 protein expression, mature sarcomere isoforms MYH7 and TNNI3 mRNA expression were significantly lowered in comparison to the control (Figure 5C).

For ion channel maturation, we evaluated mRNA expression of KCNJ2, ATPase sarcoplasmic/endoplasmic reticulum Ca2+ transporting 2 (ATP2A2, also known as SERCA2A), calcium voltage-gated channel subunit alpha1 C (CACNA1C), and sodium voltage-gated channel alpha subunit (SCN5A) (Figure 5E). ATP2A2 and CACNA1C are essential for calcium handling in cardiomyocytes, whereas SCN5A establishes the depolarizing Na+ current that results in the cardiac action potential [30–32]. All three genes are developmentally regulated since they are highly expressed in postnatal cardiomyocyte development and are key for allowing cardiac function in adults [30–32]. We observed an increase in KCNJ2 protein expression after Nutlin3a treatment that corresponded to a decrease in KNCJ2 mRNA expression after Nutlin3a treatment (Figure 5E). Furthermore, we observed no differences in mRNA expression of mature ion channels ATP2A2, CACNA1C, and SCN5A between the control and other treatments that promote maturation (Figure 5E).

Increased protein expression of KCNJ2 after Nutlin3a treatment was an indicator of electrical maturation. Therefore, we wanted to examine if the increased expression of potassium ion channels translated into contractile changes. In addition to the expression of sarcomere and electrical

maturation genes, we studied contractility by beat amplitude changes (Figure S3A) and spike amplitude changes in unpaced cells via multielectrode array (MEA) (Figure S3B). Beat amplitude and period measure maximum contraction and time for a full contraction cycle, respectively, while spike amplitude measures membrane potential resulting from ion currents.

We observed P53 activation via Nutlin3a and mTOR inhibition via Torin-1 caused significant decreases in spike amplitude (Figure 5F), while FOXO1 activation via LOM612 significantly decreased beat amplitude (Figure 5G). Both of these measures indicated a decreased action potential and contractile properties [33]. On the other hand, the beat period mean of Nutlin3a-treated iPSC-CM increased significantly in comparison to the control, which means the treated cells are beating at a slower rate than the control-treated cells. This is indicative of decreased spontaneous beating after Nutlin3a treatment that is associated with a more mature iPSC-CM [27,34]

Separate from our aim of improving iPSC-CM maturation in vitro, we observed FOXO1 inhibition via AS1842856 treatment caused a loss of iPSC-CM identity. Here, TNNT2 and other mature sarcomere genes had drastically decreased expression after AS1842856 treatment in comparison to the control treatment (Figure 5B-C). Similarly, KCNJ2 and other ion channel genes had considerably reduced expression after AS1842856 treatment in comparison to the control treatment (Figure 5D-E), suggesting FOXO1 inhibition induces a less contractile phenotype. In turn, beat and spike amplitude drastically dropped after the FOXO1 inhibition AS1842856 treatment (Figure 5F-G), suggesting FOXO1 inhibition induces a non-cardiomyocyte cell state that lacks beating.

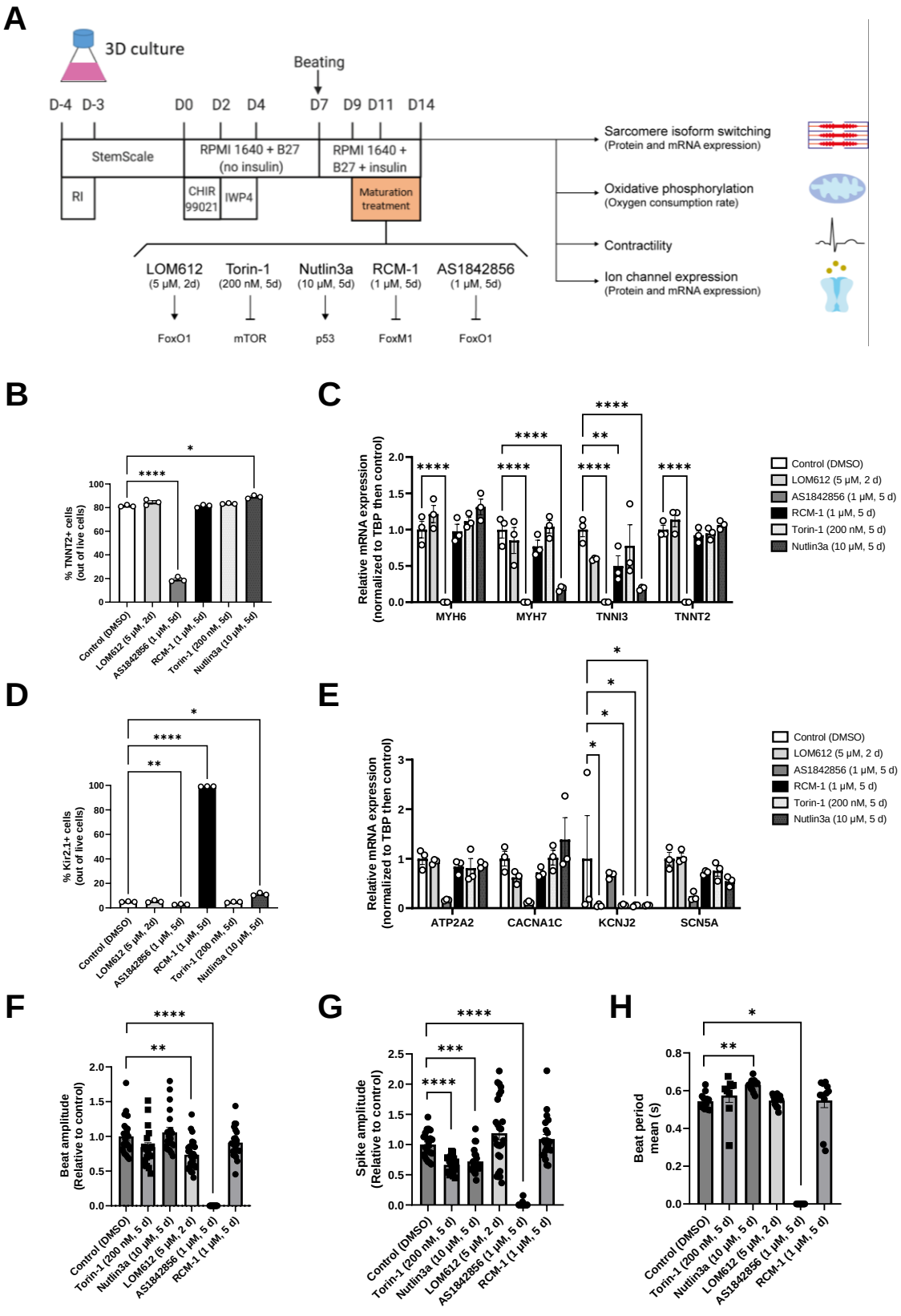
A
3D culture
Beating
D-4 D-3 D0 D2 D4 D7 D9 D11 D14
StemScale
RPMI 1640 + B27 (no insulin)
RPMI 1640 + B27 + insulin
RI
CHIR 99021
IWP4
Maturation treatment
LOM612 (5 μM, 2d)
Torin-1 (200 nM, 5d)
Nutlin3a (10 μM, 5d)
RCM-1 (1 μM, 5d)
AS1842856 (1 μM, 5d)
FoxO1
mTOR
p53
FoxM1
FoxO1
Sarcomere isoform switching (Protein and mRNA expression)
Oxidative phosphorylation (Oxygen consumption rate)
Contractility
Ion channel expression (Protein and mRNA expression)
B
% TNNT2+ cells (out of live cells)
C
Relative mRNA expression (normalized to TBP then control)
MYH6
MYH7
TNNI3
TNNT2
Control (DMSO)
LOM612 (5 μM, 2 d)
AS1842856 (1 μM, 5 d)
RCM-1 (1 μM, 5 d)
Torin-1 (200 nM, 5 d)
Nutlin3a (10 μM, 5 d)
D
% Kir2.1+ cells (out of live cells)
E
Relative mRNA expression (normalized to TBP then control)
ATP2A2
CACNA1C
KCNJ2
SCN5A
F
Beat amplitude (Relative to control)
G
Spike amplitude (Relative to control)
H
Beat period mean (s)

Figure 5. Nutlin3a P53 activation and RCM-1 FOXM1 inhibition show the most significant changes in cardiac muscle and ion channel expression in iPSC-CM after day 9 of differentiation. (A) Schematic representation of soluble factor maturation treatment at day 9 of differentiation in 3D iPSC-CM cultures for comparison of maturation readouts by protein expression via FACS, gene expression via qPCR, contractility via MEA, and oxygen consumption rate via seahorse XF cell mito stress test. (B) Percentage of TNNT2 expressing cells and (D) percentage of Kir2.1 expressing cells after soluble factor treatments starting at day 9 by flow cytometry. *p<0.05, **p<0.005, ****p<0,0001 by one-way ANOVA with Brown-Forsythe and Welch multiple comparison analysis compared to the control treatment (n=3 samples per condition, plotted as mean +/- SEM). (C) Relative mRNA expression of cardiac muscle genes and (E) ion channel genes by qPCR after maturation treatments starting at day 9 of iPSC-CM differentiation, normalized to TBP and then to control DMSO treatment. *p<0.05, **p<0.005, ***p<0,0005, ****p<0,0001 by two-way ANOVA with Dunnett's multiple comparison test compared to the control treatment (n=3 samples per condition). (F) Contractility parameters beat amplitude, and (G) spike amplitude calculated by multielectrode array analysis relative to control DMSO treatment. *p<0.05, **p<0.005, ***p<0,0005, ****p<0,0001 by one-way ANOVA with Kruskal-Wallis multiple comparison analysis compared to the control treatment (n=26 wells from 5 samples per condition, plotted as mean +/- SEM). (H) Beat period calculated in seconds (s) by multielectrode array analysis. *p<0.05, **p<0.005 by one-way ANOVA with Kruskal-Wallis multiple comparison analysis compared to the control treatment (n=15 wells from 3 samples per condition, plotted as mean +/- SEM).

P53 activation is comparable to FOXO1 activation at inducing metabolic changes in iPSC-CM.

P53 activation via Nutlin3a treatment significantly improved iPSC-CM maturation in terms of contractility, and sarcomere and ion channel expression when compared to other established soluble factor methods. Hereafter, we compared metabolic maturation changes in different soluble factor treatments via the Seahorse XF cell mito stress test (Figure S2A, S2B). We analyzed the different soluble factor treatments on day 9 of differentiation by measuring the oxygen consumption rate and bioenergetic parameters related to cellular respiration (Figure 5A). Nutlin3a had a significant increase in oxygen consumption rate across the different bioenergetic parameters (Basal respiration, ATP-linked respiration, maximal respiration, respiratory reserve capacity, and non-mitochondrial respiration) (Figure 6C-D). Similarly, FOXO1 activation also significantly increased all bioenergetic parameters (Figure 6E-F), and mTOR inhibition and FOXM1 inhibition slightly increased the oxygen consumption rate of some bioenergetic parameters (Figure 6A-B, 6I-J).

In accordance with our previous results, AS1842856 treatment resulted in drastically different cell phenotypes in comparison to other treatments that promoted iPSC-CM maturation. AS1842856 significantly decreased all bioenergetic parameters related to oxidative phosphorylation (Basal respiration, ATP-linked respiration, maximal respiration, and respiratory reserve capacity) (Figure 6G-H). Interestingly, non-mitochondrial respiration increased significantly after AS1842856 treatment, suggesting inhibiting FOXO1 induces a cell phenotype with decreased cellular respiration rates in comparison to iPSC-CM. Therefore, FOXO1 inhibition via AS1842856 induced a non-cardiomyocyte cell state that lacks beating and has decreased cellular respiration.

Our analysis of different iPSC-CM maturation methods showed P53 activation and FOXO1 activation increased oxidative respiration in comparison to mTOR inhibition and FOXM1 inhibition after 9 days of differentiation. Likewise, P53 activation also increased the expression of cardiac muscle and ion channels, suggesting Nutlin3a treatment achieves better maturation in 3D iPSC-CM compared to other soluble factors.

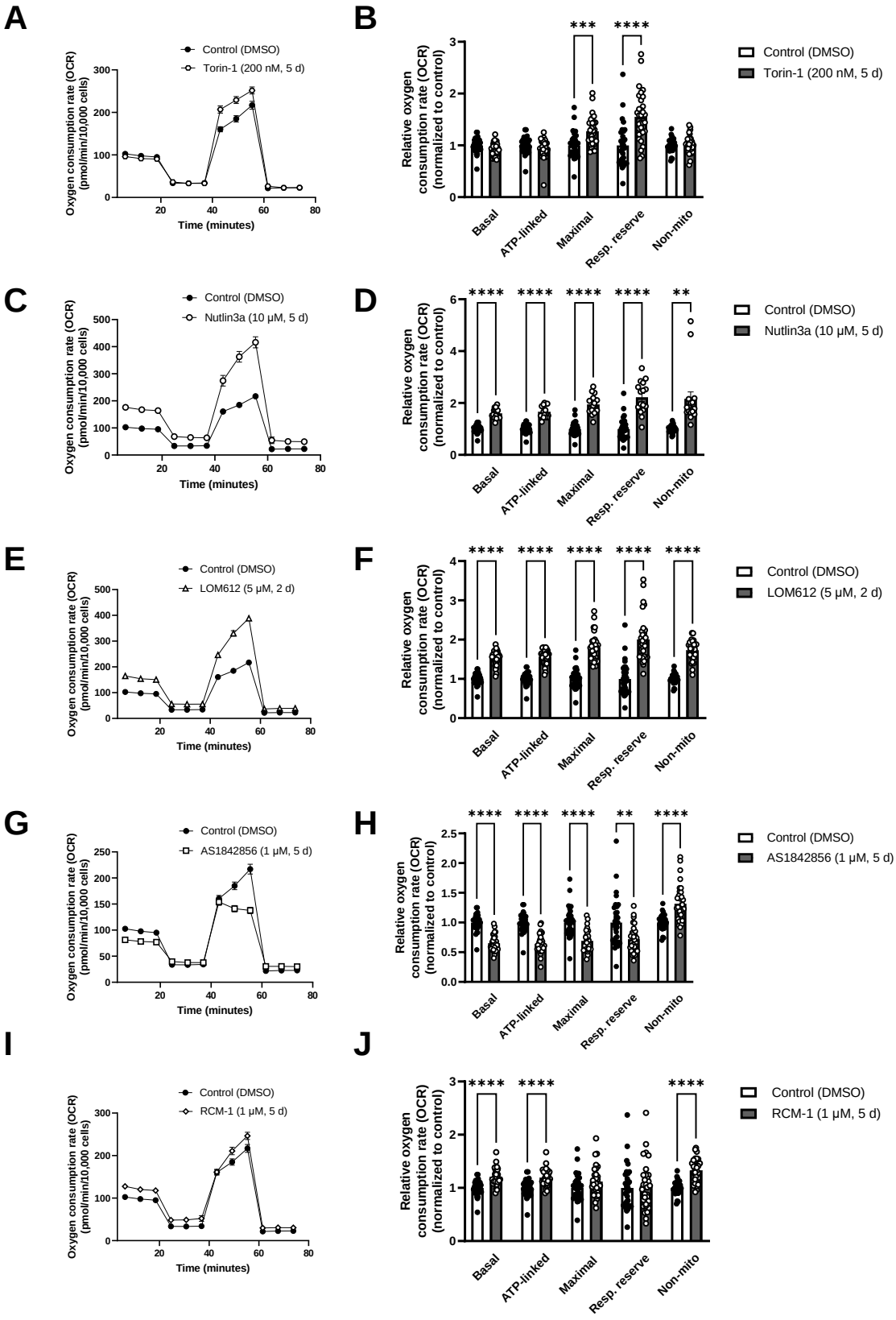
A
Control (DMSO)
Torin-1 (200 nM, 5 d)
Oxygen consumption rate (OCR) (pmol/min/10,000 cells)
Time (minutes)
B
Relative oxygen consumption rate (OCR) (normalized to control)
Basal
ATP-linked
Maximal
Resp. reserve
Non-mito
C
Nutlin3a (10 μM, 5 d)
D
E
LOM612 (5 μM, 2 d)
F
G
AS1842856 (1 μM, 5 d)
H
I
RCM-1 (1 μM, 5 d)
J

Figure 6. Nutlin3a P53 activation is comparable to LOM612 FOXO1 activation at inducing metabolic changes in iPSC-CM after day 9 of differentiation. (A) Oxygen consumption rate profile and (B) oxygen consumption rate parameters after Torin-1 treatment starting at day 9 of differentiation, measured by Seahorse XF cell mito stress test and normalized to control DMSO treatment. (C) Oxygen consumption rate profile and (D) oxygen consumption rate parameters after Nutlin3a treatment starting at day 9 of differentiation, measured by Seahorse XF cell mito stress test and normalized to control DMSO treatment. (E) Oxygen consumption rate profile and (F) oxygen consumption rate parameters after LOM612 treatment starting at day 9 of differentiation, measured by Seahorse XF cell mito stress test and normalized to control DMSO treatment. (G) Oxygen consumption rate profile and (H) oxygen consumption rate parameters after AS1842856 treatment starting at day 9 of differentiation, measured by Seahorse XF cell mito stress test and normalized to control DMSO treatment. (I) Oxygen consumption rate profile and (J) oxygen consumption rate parameters after RCM-1 treatment starting at day 9 of differentiation, measured by Seahorse XF cell mito stress test and normalized to control DMSO treatment. *p<0.05, **p<0.005, ***p<0,0005, ****p<0,0001 by one-way ANOVA with Brown-Forsythe and Welch multiple comparison analysis compared to the control treatment (DMSO n=32 wells from 2 samples, Torin-1 n=32 wells from 2 samples, Nutlin3a n=16 wells from 2 samples, LOM612 n=32 wells from 2 samples, AS1842856 n=32 wells from 2 samples, RCM-1 n=32 wells from 2 samples, plotted as mean +/- SEM).

Combinatorial soluble factor treatment: mTOR inhibition and P53 activation treatment showed an increase in oxygen consumption rate.

Our results suggested P53 activation improved iPSC-CM maturation significantly after comparing the effects of different soluble factor treatments. To further improve our maturation protocol, we tested if combinatorial treatments would further improve iPSC-CM maturation compared to single treatments after 9 days of iPSC-CM differentiation. To include additional pathways of maturation, we also included the soluble factor AICAR, 5' adenosine monophosphate-activated protein kinase (AMPK) activator into the combinatorial treatments (Figure S5A). AMPK regulates metabolism by increasing fatty acid uptake and was shown to induce early differentiation in iPSC-CM [35]. Thus, we combined soluble factors Nutlin3a, Torin-1, LOM612, RCM-1, and AICAR in different double, triple, and quadruple maturation treatments (Figure 7A)

Here, we tested eleven different soluble factor combinations and we screened for mRNA expression of sarcomere and ion channel genes by qPCR (Figure 7, S5). Among these combinations, Nutlin3a + Torin-1 treatment significantly increased fetal isoform MYH6 expression and decreased post-natal isoform MYH7 expression, indicating sarcomere maturation was not improved (Figure 7B). All other combinations did not induce significant changes in the expression of sarcomere or ion channel expression (Figure S5). However, the Nutlin3a + Torin-1 combination significantly increased KCNJ2 expression, even when compared to single Nutlin3a and Torin-1 treatments (Figure 7C).

Furthermore, we followed the results of the Nutlin3a + Torin1 combination by measuring metabolic changes via Seahorse XF cell mito stress test. Here, we found that Nutlin3a + Torin-1 significantly increased all bioenergetic parameters (Basal respiration, ATP-linked respiration, maximal respiration, and respiratory reserve capacity) (Figure 7D-E). Therefore, our results suggested combination treatments can still further improve iPSC-CM ion channel and metabolic maturation in comparison to single treatments.

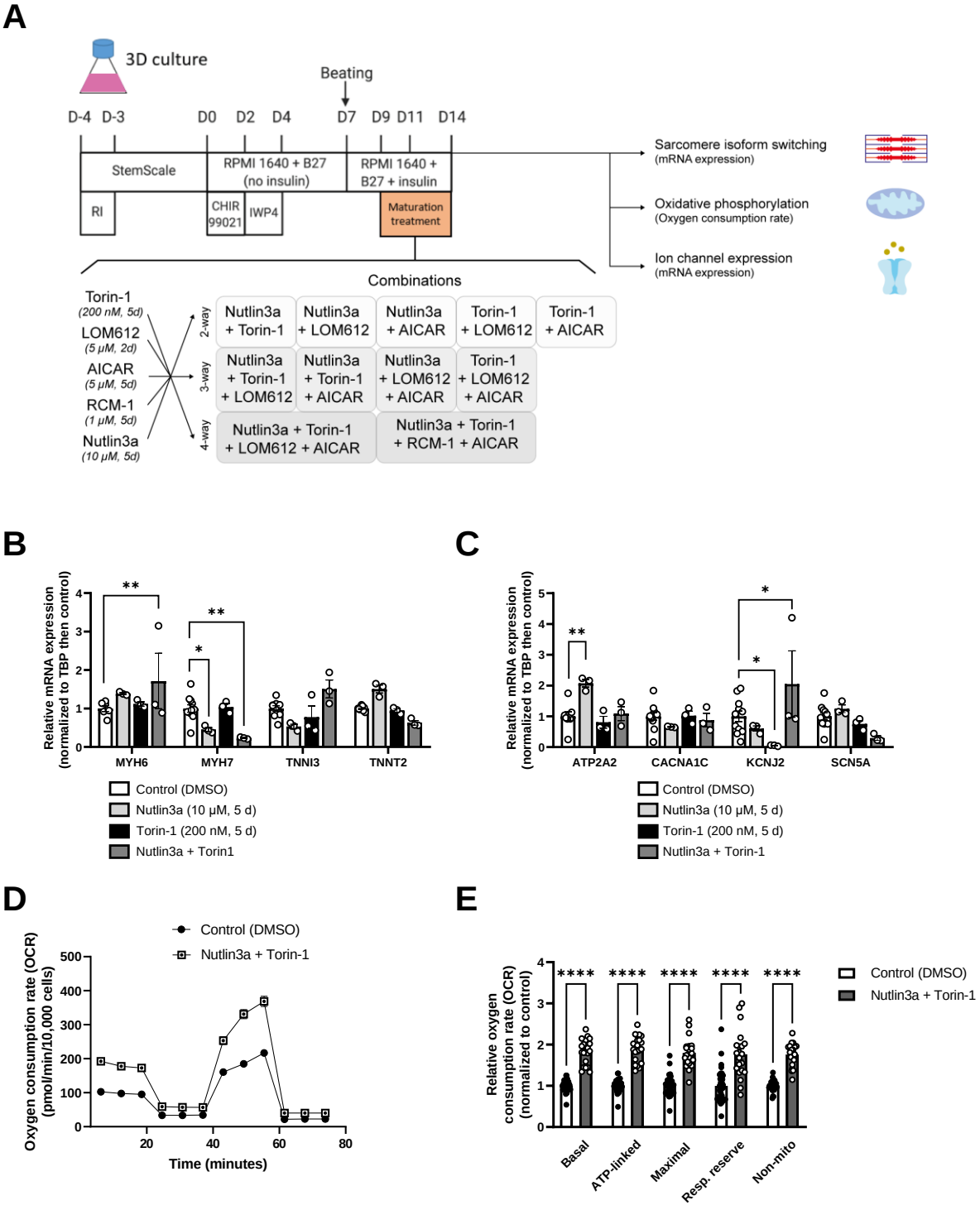
A
3D culture
Beating
D-4 D-3 D0 D2 D4 D7 D9 D11 D14
StemScale
RPMI 1640 + B27 (no insulin)
RPMI 1640 + B27 + insulin
RI
CHIR 99021
IWP4
Maturation treatment
Sarcomere isoform switching (mRNA expression)
Oxidative phosphorylation (Oxygen consumption rate)
Ion channel expression (mRNA expression)
Combinations
Torin-1 (200 nM, 5d)
LOM612 (5 μM, 2d)
AICAR (5 μM, 5d)
RCM-1 (1 μM, 5d)
Nutlin3a (10 μM, 5d)
2-way
3-way
4-way
Nutlin3a + Torin-1
Nutlin3a + LOM612
Nutlin3a + AICAR
Torin-1 + LOM612
Torin-1 + AICAR
Nutlin3a + Torin-1 + LOM612
Nutlin3a + Torin-1 + AICAR
Nutlin3a + LOM612 + AICAR
Torin-1 + LOM612 + AICAR
Nutlin3a + Torin-1 + LOM612 + AICAR
Nutlin3a + Torin-1 + RCM-1 + AICAR
B
Relative mRNA expression (normalized to TBP then control)
MYH6
MYH7
TNNI3
TNNT2
Control (DMSO)
Nutlin3a (10 μM, 5 d)
Torin-1 (200 nM, 5 d)
Nutlin3a + Torin1
C
Relative mRNA expression (normalized to TBP then control)
ATP2A2
CACNA1C
KCNJ2
SCN5A
Control (DMSO)
Nutlin3a (10 μM, 5 d)
Torin-1 (200 nM, 5 d)
Nutlin3a + Torin-1
D
Control (DMSO)
Nutlin3a + Torin-1
Oxygen consumption rate (OCR) (pmol/min/10,000 cells)
Time (minutes)
E
Relative oxygen consumption rate (OCR) (normalized to control)
Basal
ATP-linked
Maximal
Resp. reserve
Non-mito
Control (DMSO)
Nutlin3a + Torin-1

Figure 7. Combinatorial Torin-1 mTOR inhibition and Nutlin3a P53 activation treatment showed an increase in KCNJ2 expression and oxygen consumption rate. (A) Schematic representation of combinatorial soluble factor maturation treatment at day 9 of differentiation in 3D iPSC-CM cultures for comparison of maturation readouts by gene expression via qPCR, and oxygen consumption rate via seahorse XF cell mito stress test. (B) Relative mRNA expression of cardiac muscle genes and (C) ion channel genes by qPCR after combinatorial maturation treatment starting at day 9 of iPSC-CM differentiation, normalized to TBP and then to control DMSO treatment. *p<0.05, **p<0.005 by two-way ANOVA with Dunnett's multiple comparison test compared to the control treatment (DMSO n=11 samples, Torin-1 n=3 samples, Nutlin3a n=3 samples, Nutlin3a + Torin-1 n=3 samples, plotted as mean +/- SEM). (D) Oxygen consumption rate profile and (E) oxygen consumption rate parameters after combinatorial maturation treatment starting at day 9 of differentiation, measured by Seahorse XF cell mito stress test and normalized to control DMSO treatment. ****p<0,0001 by one-way ANOVA with Brown-Forsythe and Welch multiple comparison analysis compared to the control treatment (DMSO n=32 wells from 2 samples, Nutlin3a + Torin-1 n=21 wells from 3 samples, plotted as mean +/- SEM).

Discussion

Our study aimed to improve iPSC-CM maturation with the later purpose of avoiding life-threatening arrhythmias after transplantation. We followed up on previous results that studied the iPSC-CM maturation by inducing postnatal signaling switches with soluble factors [13]. Namely, we continued studying the mTOR inhibition and P53 activation pathway that led to expression changes in FOXO1 activation and FOXM1 inhibition, involved in neonatal CM quiescence [19.]

Our results showed the maturation effects of FOXO1 activation and FOXM1 inhibition were enhanced at later time points of differentiation. Similar to other studies, a longer time in culture improved baseline iPSC-CM maturation in our 50-day differentiation of iPSC-CM [36]. Therefore, we showed iPSC-CM in prolonged 3D cultures were still responsive to the FOXO1/FOXM1 maturation pathway, suggesting a new way to improve iPSC-CM maturation in vitro.

Following our study of prolonged cultures, we compared the effects of different soluble factor treatments on iPSC-CM maturation in 3D cultures. We identified an increase in TNNT2 expression after P53 activation that, like other studies, is indicative of iPSC-CM maturation and myocyte identity [25]. However, common post-natal sarcomere genes such as TNNI3 and MYH7 were expressed at similar levels in all soluble factor treatments, indicating further improvement is needed to resemble post-natal CM sarcomere expression in our iPSC-CM maturation method.

Furthermore, we found a significant increase in potassium ion channel KCNJ2 expression after P53 induction and, especially after FOXM1 inhibition. Therefore, we expected this increased KCNJ2 expression to translate to contractile changes. We observed an increased beat period after P53 activation in our data. This meant there is less spontaneous beating after P53 activation, which is associated with iPSC-CM maturity [27,34]. However, our results show a decreased spike amplitude after P53 activation, indicative of a lower ion current and decreased contractile properties [33]. Together, our ion channel expression data and the multielectrode array data showed relevant iPSC-CM maturation after P53 activation.

Lastly, we found both P53 activation and FOXO1 activation are comparable in inducing metabolic maturation in iPSC-CM by increasing rates of oxidative respiration. These metabolic changes represent the postnatal CM switch from anaerobic glycolysis to oxidative phosphorylation during CM development [37]. In addition, increasing rates of oxidative respiration were reported in other iPSC-CM maturation protocols as a benchmark of CM maturation [37].

Taken together, we demonstrated the FOXO1/FOXM1 pathway further contributes to iPSC-CM maturation in 3D, and was also inducible in prolonged cultures. FOXO1 activation/FOXM1 inhibition is thus a novel iPSC-CM maturation pathway. However, when compared to other maturation methods, upstream P53 induction induced more sarcomere, contractile, and metabolic maturation than other soluble factor treatments such as mTOR inhibition and FOXO1/FOXM1 alterations. Besides this, FOXO1 inhibition via AS1842856 induced a non-cardiomyocyte cell

state that lacks beating and has decreased cellular respiration, as opposed to inducing iPSC-CM maturation via FOXO1 activation. Exploring the FOXO1 inhibition effects on inducing an alternative differentiation after iPSC-CM is a future direction for an alternative research question.

Interestingly, further combining P53 activation with mTOR inhibition improved iPSC-CM maturation in 3D, representing a new biochemical iPSC-CM maturation strategy. In comparison to single P53 activation and mTOR inhibition treatments, this combination resulted in increased KCNJ2 expression and increased oxidative respiration. Other studies have identified novel combinations of biochemical signals that create a coordinated CM maturation program. Examples of these include thyroid hormone T3 + Dexamethasone in hiPSC-CM [9], T3 + Dexamethasone + Insulin-like growth factor 1 (IGF1) in hiPSC-CM [38], T3 + IGF1 in E18 rat CM [39], and HIF-1a inhibition + PPARa activation in hiPSC-CM [40]. Similarly, we identified a new synergy of biochemical signaling that promotes iPSC-CM maturation in 3D by combining P53 activation and mTOR inhibition.

Despite P53 activation and FOXM1 inhibition improving iPSC-CM maturation individually, combining these two treatments did not result in improved iPSC-CM maturation. We hypothesized this occurred because of the complexity of interactions between signaling pathways. For example, the Ras-Raf-MEK-ERK [41], and mTOR-IGF [42] pathway interactions rely on complex fine-tuning to dictate specific biological outputs. We propose studying the signaling pathway synergies between P53 activation and FOXM1 inhibition in 3D culture via differential gene expression analysis. This could be achieved, for example, by employing bulk RNA sequencing after single and combined biochemical treatments. Here, we could characterize the P53 and FOXM1 pathways of iPSC-CM maturation in detail. In addition, we could further identify specific components necessary for fine-tuning the P53-FOXM1 pathway synergy and biochemically target these components during iPSC-CM maturation. We believe studying the details of the P53-FOXM1 signaling pathway is a potential way of improving current iPSC-CM maturation methods.

In conclusion, we show new maturation methods that recapitulate some CM maturation not present in previous studies. Our method leverages 3D culture and biochemical signaling to facilitate opportunities for upscaling of iPSC-CM differentiation in clinical approaches. The future direction for this research is to study the effect of FOXM-1 inhibition on inducing ion channel expression in iPSC-CM. Furthermore, we hypothesize studying the biochemical synergy between FOXM1 inhibition and P53 activation will yield improved sarcomere, metabolic, and contractile maturation. Successful clinical applicability is reliant on improved electrophysiological characteristics of iPSC-CM, thus adding methods like patch-clamping, sharp electrode measurements, or voltage sensitive-fluorescence would give us a more complete indication of action potentials in our iPSC-CM [43]. Ultimately, clinically applicable iPSC-CM maturation protocols would need to achieve tissue-like action potentials before moving to small and large animal model testing of iPSC-CM transplantation. Reaching this benchmark of CM maturation will answer our hypothesis of overcoming arrhythmias in large animal model transplantation.

Acknowledgments

I would like to thank Prof. Richard T. Lee and Dr. Nivedhitha Velayutham for their guiding input and feedback during this project. Furthermore, I want to thank Laura Ruland, Elisabeth Ricci-Blair, Jeanna Shaw, Alex Kreymerman, the FACS SCRB core at Harvard University, and the rest of the Richard T. Lee Lab for their helpful contributions and practical support. Besides this, I would like to acknowledge the previous work of Jessica Garbern and Hannah Elwell that contributed to the start of this project. Finally, I would like to thank Prof. Joost Sluijter for serving as my reviewer and the U/SELECT program for sponsoring this project, as well as my family, my partner, and my friends for their continuous support during this project.

References

1. Khan, M. A. *et al.* Global epidemiology of ischemic heart disease: Results from the Global Burden of disease study. *Cureus* **12**, e9349 (2020).

2. Shiba, Y. *et al.* Allogeneic transplantation of iPS cell-derived cardiomyocytes regenerates primate hearts. *Nature* **538**, 388–391 (2016).

3. Chong, J. J. H. *et al.* Human embryonic-stem-cell-derived cardiomyocytes regenerate non-human primate hearts. *Nature* **510**, 273–277 (2014).

4. Romagnuolo, R. *et al.* Human embryonic stem cell-derived cardiomyocytes regenerate the infarcted pig heart but induce ventricular tachyarrhythmias. *Stem Cell Reports* **12**, 967–981 (2019).

5. Caspi, O. *et al.* Transplantation of Human Embryonic Stem Cell-Derived Cardiomyocytes Improves Myocardial Performance in Infarcted Rat Hearts. *J Am Coll Cardiol* **50**, 1884–1893 (2007).

6. Guo, Y. & Pu, W. T. Cardiomyocyte Maturation. *Circ Res* **126**, 1086–1106 (2020).

7. Zhao, M.-T., Ye, S., Su, J. & Garg, V. Cardiomyocyte Proliferation and Maturation: Two Sides of the Same Coin for Heart Regeneration. *Front Cell Dev Biol* **8**, (2020).

8. Yang, X. *et al.* Tri-iodo-l-thyronine promotes the maturation of human cardiomyocytes-derived from induced pluripotent stem cells. *J. Mol. Cell. Cardiol.* **72**, 296–304 (2014).

9. Parikh, S. S. *et al.* Thyroid and glucocorticoid hormones promote functional T-tubule development in human-induced pluripotent stem cell-derived cardiomyocytes. *Circ. Res.* **121**, 1323–1330 (2017).

10. Yang, X. *et al.* Fatty acids enhance the maturation of cardiomyocytes derived from human pluripotent stem cells. *Stem Cell Reports* **13**, 657–668 (2019).

11. Wang, L. *et al.* Triiodothyronine and dexamethasone alter potassium channel expression and promote electrophysiological maturation of human-induced pluripotent stem cell-derived cardiomyocytes. *J Mol Cell Cardiol* **161**, 130–138 (2021).

12. Ergir, E. *et al.* Generation and maturation of human iPSC-derived 3D organotypic cardiac microtissues in long-term culture. *Sci Rep* **12**, 17409 (2022).

13. Garbern, J. C. *et al.* Inhibition of mTOR Signaling Enhances Maturation of Cardiomyocytes Derived From Human-Induced Pluripotent Stem Cells via p53-Induced Quiescence. *Circulation* **141**, 285–300 (2020).

14. Dai, D.-F., Danoviz, M. E., Wiczer, B., Laflamme, M. A. & Tian, R. Mitochondrial maturation in human pluripotent stem cell derived cardiomyocytes. *Stem Cells Int.* **2017**, 5153625 (2017).

15. Liu, A. *et al.* Functional characterization of inward rectifier potassium ion channel in murine fetal ventricular cardiomyocytes. *Cell. Physiol. Biochem.* **26**, 413–420 (2010).

16. Kubalak, S. W., Miller-Hance, W. C., O'Brien, T. X., Dyson, E. & Chien, K. R. Chamber specification of atrial myosin light chain-2 expression precedes septation during murine cardiogenesis. *J. Biol. Chem.* **269**, 16961–16970 (1994).

17. Reiser, P. J., Portman, M. A., Ning, X.-H. & Moravec, C. S. Human cardiac myosin heavy chain isoforms in fetal and failing adult atria and ventricles. *American Journal of Physiology-Heart and Circulatory Physiology* **280**, H1814–H1820 (2001).

18. Bedada, F. B. *et al.* Acquisition of a Quantitative, Stoichiometrically Conserved Ratiometric Marker of Maturation Status in Stem Cell-Derived Cardiac Myocytes. *Stem Cell Reports* **3**, 594–605 (2014).

19. Sengupta, A., Kalinichenko, V. V & Yutzey, K. E. FoxO1 and FoxM1 Transcription Factors Have Antagonistic Functions in Neonatal Cardiomyocyte Cell-Cycle Withdrawal and IGF1 Gene Regulation. *Circ Res* **112**, 267–277 (2013).

20. Chen, R. J. *et al.* Variations in glycogen synthesis in human pluripotent stem cells with altered pluripotent states. *PLoS One* **10**, e0142554 (2015).

21. Lian, X. *et al.* Directed cardiomyocyte differentiation from human pluripotent stem cells by modulating Wnt/β-catenin signaling under fully defined conditions. *Nat Protoc* **8**, 162–175 (2013).

22. Lian, X. *et al.* Robust cardiomyocyte differentiation from human pluripotent stem cells via temporal modulation of canonical Wnt signaling. *Proceedings of the National Academy of Sciences* **109**, E1848–E1857 (2012).

23. Ahmed, R. E., Anzai, T., Chanthra, N. & Uosaki, H. A Brief Review of Current Maturation Methods for Human Induced Pluripotent Stem Cells-Derived Cardiomyocytes. *Front Cell Dev Biol* **8**, (2020).

24. Wu, P. *et al.* Maturation strategies and limitations of induced pluripotent stem cell-derived cardiomyocytes. *Biosci Rep* **41**, BSR20200833 (2021).

25. Abilez, O. J. *et al.* Passive Stretch Induces Structural and Functional Maturation of Engineered Heart Muscle as Predicted by Computational Modeling. *Stem Cells* **36**, 265–277 (2018).

26. Wood, L. S., Tsai, T.-D., Lee, K. S. & Vogeli, G. Cloning and functional expression of a human gene, hIRK1, encoding the heart inward rectifier K+-channel. *Gene* **163**, 313–317 (1995).

27. Karbassi, E. *et al.* Cardiomyocyte maturation: advances in knowledge and implications for regenerative medicine. *Nat Rev Cardiol* **17**, 341–359 (2020).

28. Ye, L. *et al.* Activation of AMPK promotes maturation of cardiomyocytes derived from human induced pluripotent stem cells. *Front. Cell Dev. Biol.* **9**, 644667 (2021).

29. Lompré, A. M., Nadal-Ginard, B. & Mahdavi, V. Expression of the cardiac ventricular alpha- and beta-myosin heavy chain genes is developmentally and hormonally regulated. *J. Biol. Chem.* **259**, 6437–6446 (1984).

30. Campostrini, G. *et al.* Maturation of hiPSC-derived cardiomyocytes promotes adult alternative splicing of SCN5A and reveals changes in sodium current associated with cardiac arrhythmia. *Cardiovasc Res* **119**, 167–182 (2023).

31. Lin, J. *et al.* Cas9/AAV9-Mediated Somatic Mutagenesis Uncovered the Cell-Autonomous Role of Sarcoplasmic/Endoplasmic Reticulum Calcium ATPase 2 in Murine Cardiomyocyte Maturation. *Front Cell Dev Biol* **10**, (2022).

32. Takemura, H. *et al.* Subtype switching of L-Type Ca 2+ channel from Cav1.3 to Cav1.2 in embryonic murine ventricle. *Circ. J.* **69**, 1405–1411 (2005).

33. Harris, K. *et al.* Comparison of Electrophysiological Data From Human-Induced Pluripotent Stem Cell–Derived Cardiomyocytes to Functional Preclinical Safety Assays. *Toxicological Sciences* **134**, 412–426 (2013).

34. Lakatta, E. G., Maltsev, V. A. & Vinogradova, T. M. A Coupled SYSTEM of Intracellular Ca2+ Clocks and Surface Membrane Voltage Clocks Controls the Timekeeping Mechanism of the Heart's Pacemaker. *Circ Res* **106**, 659–673 (2010).

35. Sarikhani, M. *et al.* Sustained Activation of AMPK Enhances Differentiation of Human iPSC-Derived Cardiomyocytes via Sirtuin Activation. *Stem Cell Reports* **15**, 498–514 (2020).

36. Lewandowski, J. *et al.* The impact of in vitro cell culture duration on the maturation of human cardiomyocytes derived from induced pluripotent stem cells of myogenic origin. *Cell Transplant* **27**, 1047–1067 (2018).

37. Chirico, N. *et al.* Small molecule-mediated rapid maturation of human induced pluripotent stem cell-derived cardiomyocytes. *Stem Cell Res Ther* **13**, 531 (2022).

38. Huang, C. Y. *et al.* Enhancement of human iPSC-derived cardiomyocyte maturation by chemical conditioning in a 3D environment. *J. Mol. Cell. Cardiol.* **138**, 1–11 (2020).

39. Krüger, M. *et al.* Thyroid hormone regulates developmental titin isoform transitions via the phosphatidylinositol-3-kinase/ AKT pathway. *Circ. Res.* **102**, 439–447 (2008).

40. Gentillon, C. *et al.* Targeting HIF-1α in combination with PPARα activation and postnatal factors promotes the metabolic maturation of human induced pluripotent stem cell-derived cardiomyocytes. *J. Mol. Cell. Cardiol.* **132**, 120–135 (2019).

41. Shin, S.-Y. *et al.* Positive- and negative-feedback regulations coordinate the dynamic behavior of the Ras-Raf-MEK-ERK signal transduction pathway. *J. Cell Sci.* **122**, 425–435 (2009).

42. Yoneyama, Y. *et al.* Serine phosphorylation by mTORC1 promotes IRS-1 degradation through SCFβ-TRCP E3 ubiquitin ligase. *iScience* **5**, 1–18 (2018).

43. Casini, S., Verkerk, A. O. & Remme, C. A. Human iPSC-derived cardiomyocytes for investigation of disease mechanisms and therapeutic strategies in inherited arrhythmia syndromes: Strengths and limitations. *Cardiovasc. Drugs Ther.* **31**, 325–344 (2017).

44. Agilent Technologies. Agilent Seahorse XF Cell Mito Stress Test Kit. *https://www.agilent.com/cs/library/usermanuals/public/XF_Cell_Mito_Stress_Test_Kit_User_Guide.pdf* (2019).

45. Axion BioSystems. Cardiotoxicity and Safety: Technology, Cardiac MEA. https://www.axionbiosystems.com/applications/cardiac-activity/cardiotoxicity-and-safety#technology.

46. Axion BioSystems. iPSC-CM Contractility: High-Res Contractility. https://www.axionbiosystems.com/media/37/download?attachment.

Supplementary information

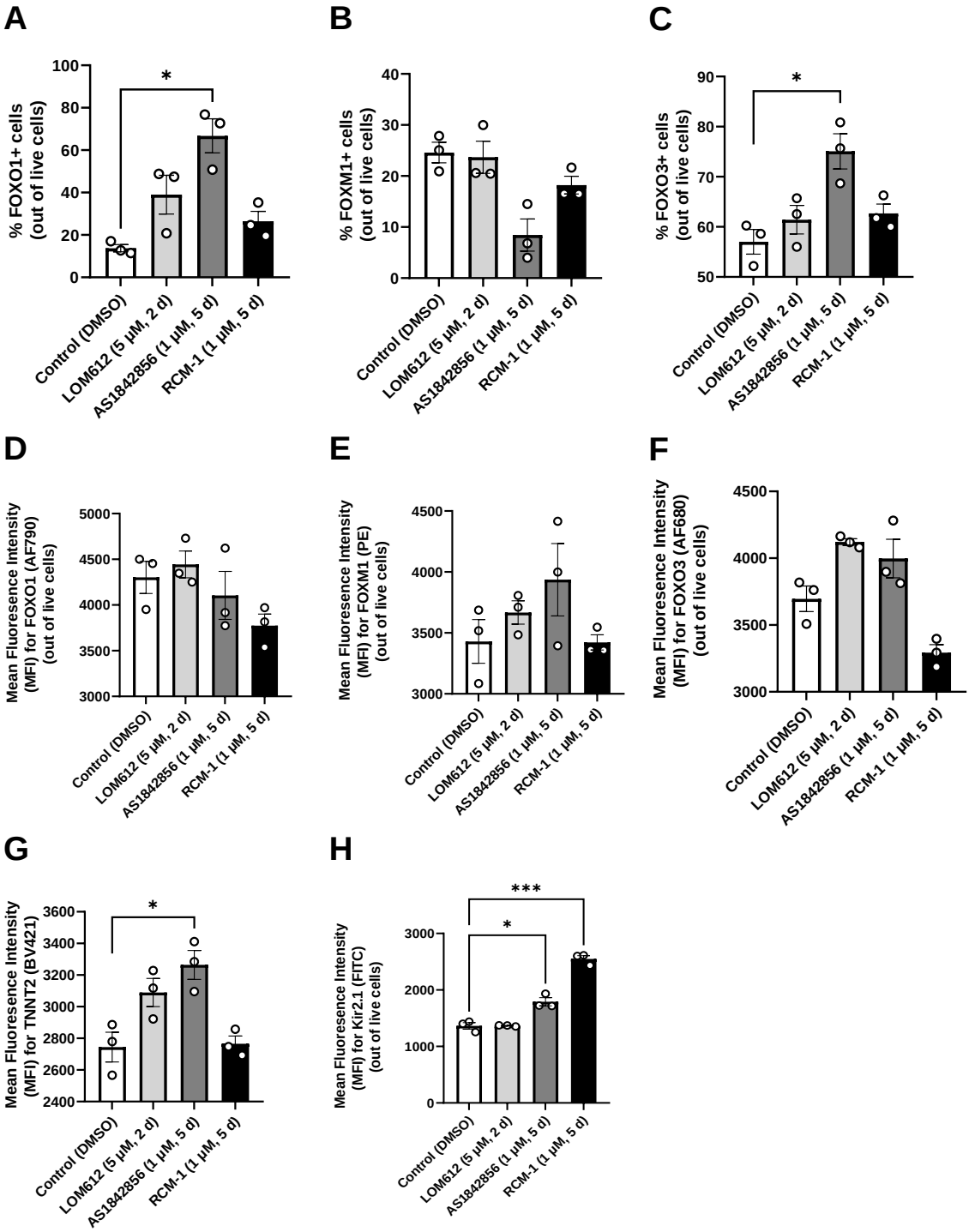

Figure S1. Extended flow cytometry data from day 45 treated iPSC-CM with FOXO1/FOXM1 altering via soluble factors. (A) Percentage of FOXO1 expressing cells and (D) mean fluorescence intensity of FOXO1-AF790 after soluble factor treatments starting at day 45 of differentiation by flow cytometry. (B) Percentage of FOXM1 expressing cells and (E) mean fluorescence intensity of FOXM1-PE after soluble factor treatments starting at day 45 of differentiation by flow cytometry. (C) Percentage of FOXO3 expressing cells and (F) mean fluorescence intensity of FOXO3-AF680 after soluble factor treatments starting at day 45 of differentiation by flow cytometry. (G) Mean fluorescence intensity of TNNT2-BV421 and (H) Kir2.1-FITC after soluble factor treatments starting at day 45 of differentiation by flow cytometry*$p<0.05$ by one-way ANOVA with Brown-Forsythe and Welch multiple comparison analysis compared to the control treatment (n=3 samples per condition, plotted as mean +/- SEM).

A

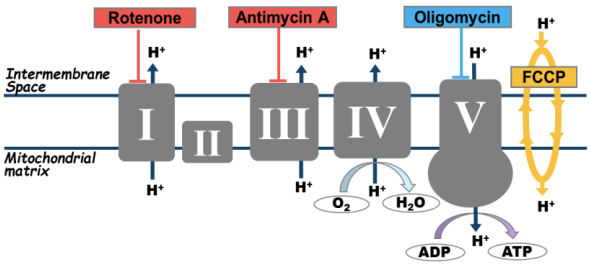

B

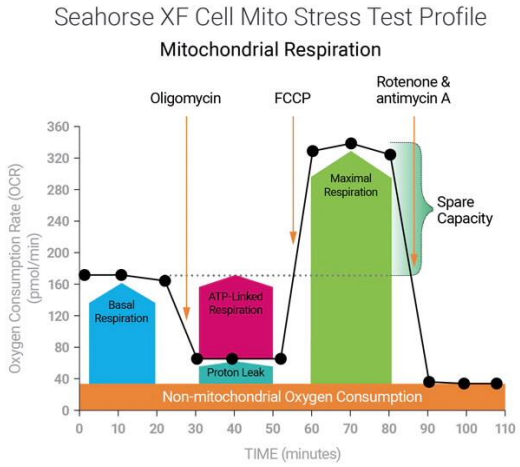

Figure S2. Schematic representation of the Agilent Seahorse XF Cell Mito Stress Test modulators and parameters taken from Agilent Technologies [44]. (A) Complexes of the electron transport chain are targeted by different modulators in the Seahorse XF Cell Mito Stress Test Kit to selectively inhibit mitochondrial function. Oligomycin inhibits ATP synthase (Complex V). Carbonyl cyanide-4 (trifluoromethoxy) phenylhydrazone (FCCP) disturbs the proton gradient and the mitochondrial membrane potential. Rotenone inhibits complex I of the electron transport chain, while antimycin inhibits complex III of the electron transport chain. Together, rotenone and antimycin A completely inhibit mitochondrial respiration. (B) Key parameters of mitochondrial function calculated based on the Agilent Seahorse XF Cell Mito Stress Test profile. Basal respiration is measured before the first modulator injection. Following the first injection with oligomycin, the decreased electron flow results in a decreased oxygen consumption rate which is indicative of ATP-linked respiration. The second injection of FCCP uninhibits electron flow through the electron transport chain and increases the oxygen consumption rate to a maximum, indicative of maximal respiration. Furthermore, the difference between basal and maximal respiration indicates the spare respiratory capacity. Finally, the third injection with rotenone and antimycin A shuts down oxygen consumption rate and is used to calculate non-mitochondrial oxygen consumption.

A

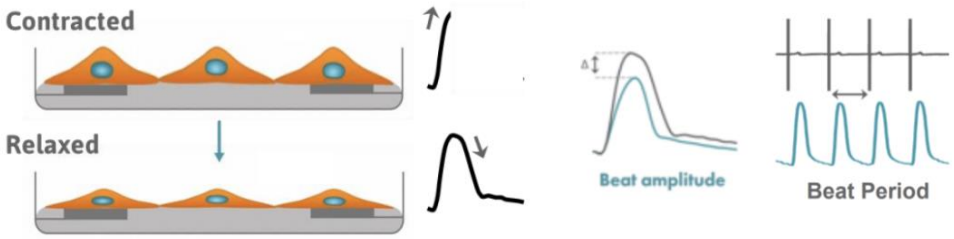

B

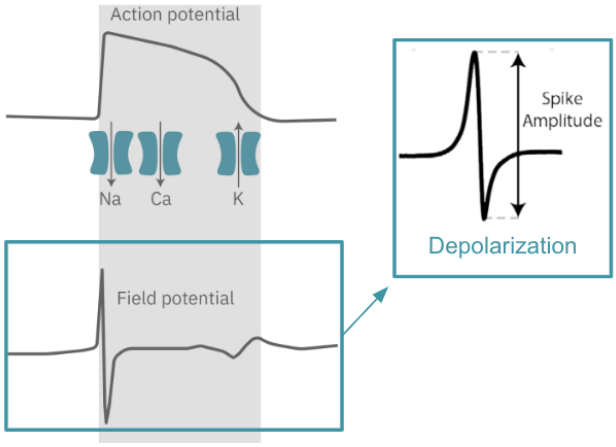

Figure S3. Schematic representation of cardiac contractility and action potential parameters taken from Axion Biosystems [45,46]. (A) iPSC-CM plated over a microelectrode array plate form a beating sheet of cells, called a syncytium. Here, a beat is a mechanical contraction resulting from the propagation of an electrical impulse. Each cell contraction and relaxation cause a change in cell shape and electrode coverage. Impedance or opposition to electrical flow is recorded by each electrode as contractility. Contraction is detected as an increase in impedance, and relaxation is detected as a decrease in impedance. Beat amplitude is measured as the difference in contractility between the maximum contraction and minimum relaxation, while the beat period is the time elapsed between a full cycle of contraction and relaxation [46] (B) The propagation of electrical impulses during beating can also be measured as a cardiac action potential, a measurement of membrane potential resulting from specific ion currents. When one iPSC-CM fires an action potential, this electrical signal propagates across the syncytium causing each iPSC-CM in the syncytium to fire and contract. This action potential propagation from cell to cell is measured by the electrodes as an extracellular field potential. The field potential is characterized by a depolarization phase seen as a sharp spike and the repolarization phase seen as a small slow spike. The depolarization spike amplitude can be calculated as a measure of membrane potential resulting from ion currents [45].

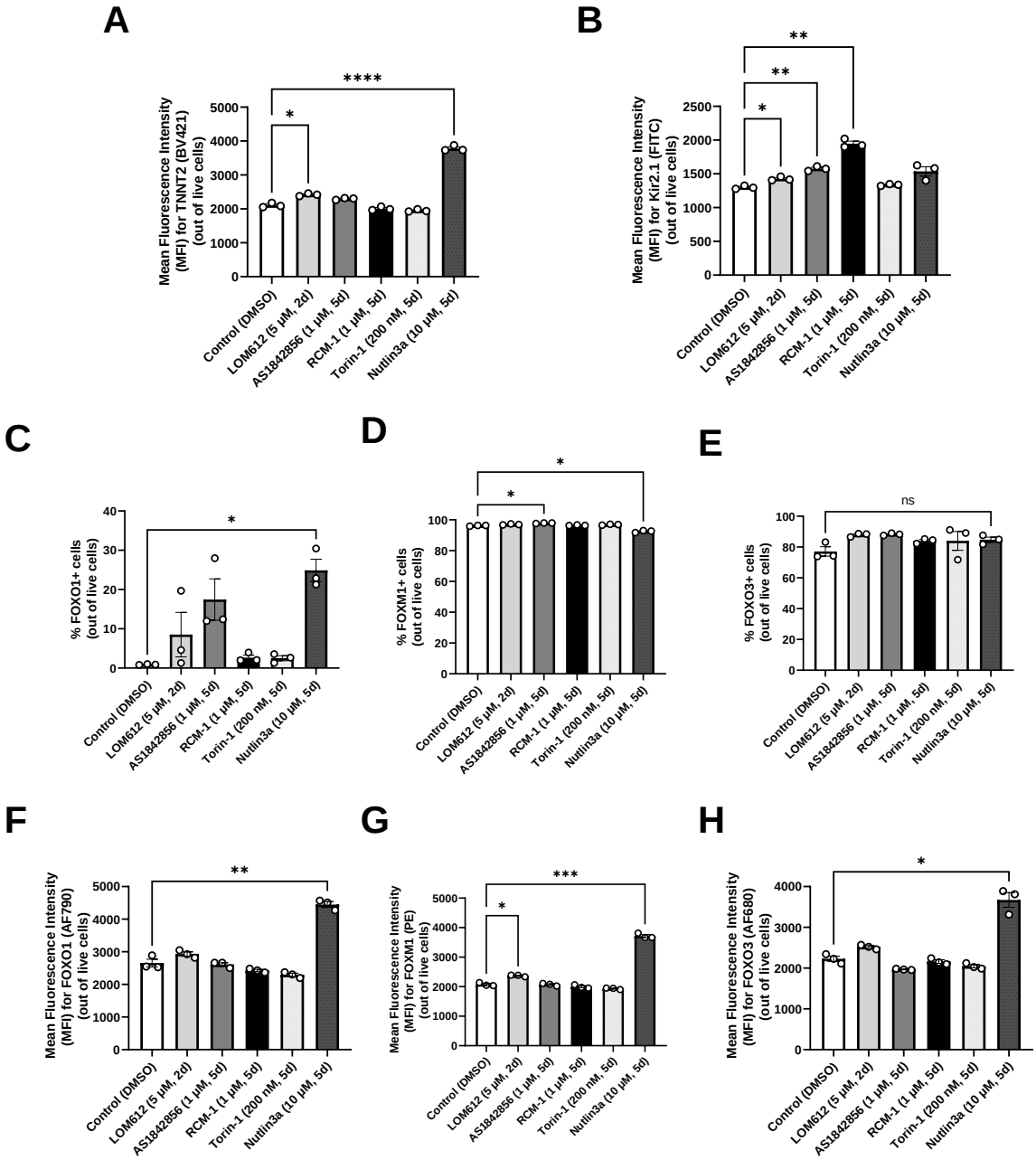
A
Mean Fluorescence Intensity (MFI) for TNNT2 (BV421) (out of live cells)
5000
4000
3000
2000
1000
0
*
****
Control (DMSO)
LOM612 (5 µM, 2d)
AS1842856 (1 µM, 5d)
RCM-1 (1 µM, 5d)
Torin-1 (200 nM, 5d)
Nutlin3a (10 µM, 5d)
B
Mean Fluorescence Intensity (MFI) for Kir2.1 (FITC) (out of live cells)
2500
2000
1500
1000
500
0
*
**
**
Control (DMSO)
LOM612 (5 µM, 2d)
AS1842856 (1 µM, 5d)
RCM-1 (1 µM, 5d)
Torin-1 (200 nM, 5d)
Nutlin3a (10 µM, 5d)
C
% FOXO1+ cells (out of live cells)
40
30
20
10
0
*
Control (DMSO)
LOM612 (5 µM, 2d)
AS1842856 (1 µM, 5d)
RCM-1 (1 µM, 5d)
Torin-1 (200 nM, 5d)
Nutlin3a (10 µM, 5d)
D
% FOXM1+ cells (out of live cells)
100
80
60
40
20
0
*
*
Control (DMSO)
LOM612 (5 µM, 2d)
AS1842856 (1 µM, 5d)
RCM-1 (1 µM, 5d)
Torin-1 (200 nM, 5d)
Nutlin3a (10 µM, 5d)
E
% FOXO3+ cells (out of live cells)
100
80
60
40
20
0
ns
Control (DMSO)
LOM612 (5 µM, 2d)
AS1842856 (1 µM, 5d)
RCM-1 (1 µM, 5d)
Torin-1 (200 nM, 5d)
Nutlin3a (10 µM, 5d)
F
Mean Fluorescence Intensity (MFI) for FOXO1 (AF790) (out of live cells)
5000
4000
3000
2000
1000
0
**
Control (DMSO)
LOM612 (5 µM, 2d)
AS1842856 (1 µM, 5d)
RCM-1 (1 µM, 5d)
Torin-1 (200 nM, 5d)
Nutlin3a (10 µM, 5d)
G
Mean Fluorescence Intensity (MFI) for FOXM1 (PE) (out of live cells)
5000
4000
3000
2000
1000
0
*
***
Control (DMSO)
LOM612 (5 µM, 2d)
AS1842856 (1 µM, 5d)
RCM-1 (1 µM, 5d)
Torin-1 (200 nM, 5d)
Nutlin3a (10 µM, 5d)
H
Mean Fluorescence Intensity (MFI) for FOXO3 (AF680) (out of live cells)
4000
3000
2000
1000
0
*
Control (DMSO)
LOM612 (5 µM, 2d)
AS1842856 (1 µM, 5d)
RCM-1 (1 µM, 5d)
Torin-1 (200 nM, 5d)
Nutlin3a (10 µM, 5d)

Figure S4. Extended flow cytometry data of in iPSC-CM at day 9 of differentiation treated with different soluble factor-based maturation treatments. (A) Mean fluorescence intensity of TNNT2-BV421 staining and (B) Kir2.1-FITC staining after soluble factor treatments starting at day 9 of differentiation by flow cytometry. (C) Percentage of FOXO1 expressing cells and (F) mean fluorescence intensity of FOXO1-AF790 after soluble factor treatments starting at day 9 of differentiation by flow cytometry. (D) Percentage of FOXM1 expressing cells and (G) mean fluorescence intensity of FOXM1-PE after soluble factor treatments starting at day 9 of differentiation by flow cytometry. (E) Percentage of FOXO3 expressing cells and (H) mean fluorescence intensity of FOXO3-AF680 after soluble factor treatments starting at day 9 of differentiation by flow cytometry. *p<0.05, **p<0.005, ***p<0,0005, ****p<0,0001 by one-way ANOVA with Brown-Forsythe and Welch multiple comparison analysis compared to the control treatment (n=3 samples per condition, plotted as mean +/- SEM).

A

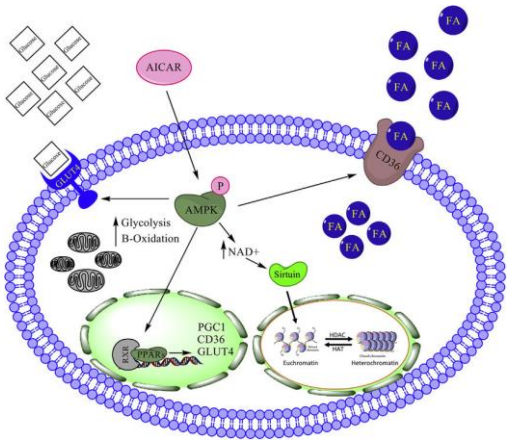
AICAR
AMPK
P
Glycolysis
B-Oxidation
NAD+
Sirtuin
PGC1
CD36
GLUT4
PPAR
FA
CD36
GLUT4
Euchromatin
Heterochromatin

B

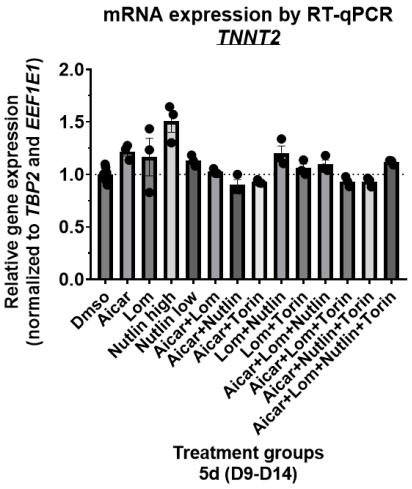
mRNA expression by RT-qPCR
TNNT2
Relative gene expression
(normalized to TBP2 and EEF1E1)
2.0
1.5
1.0
0.5
0.0
Dmso
Aicar
Lom
Nutlin high
Nutlin low
Aicar+Lom
Aicar+Nutlin
Aicar+Torin
Lom+Nutlin
Lom+Torin
Aicar+Lom+Nutlin
Aicar+Lom+Torin
Aicar+Nutlin+Torin
Aicar+Lom+Nutlin+Torin
Treatment groups
5d (D9-D14)

C

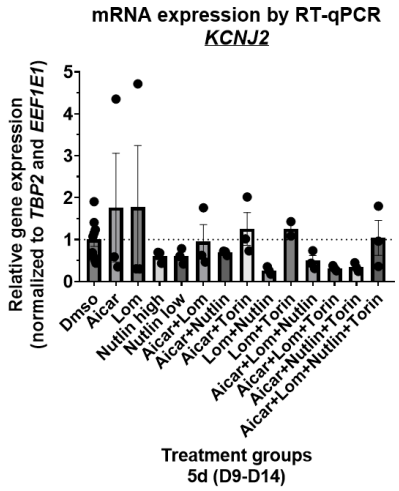
mRNA expression by RT-qPCR
KCNJ2
Relative gene expression
(normalized to TBP2 and EEF1E1)
5
4
3
2
1
0
Dmso
Aicar
Lom
Nutlin high
Nutlin low
Aicar+Lom
Aicar+Nutlin
Aicar+Torin
Lom+Nutlin
Lom+Torin
Aicar+Lom+Nutlin
Aicar+Lom+Torin
Aicar+Nutlin+Torin
Aicar+Lom+Nutlin+Torin
Treatment groups
5d (D9-D14)

D

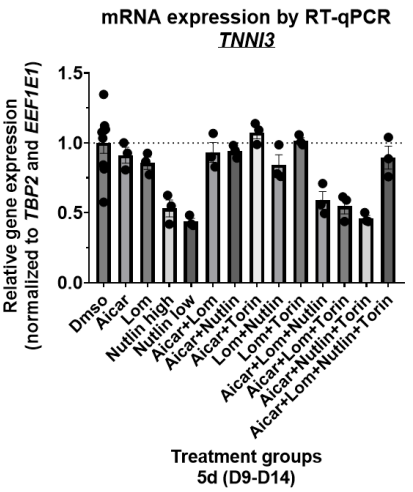
mRNA expression by RT-qPCR
TNNI3
Relative gene expression
(normalized to TBP2 and EEF1E1)
1.5
1.0
0.5
0.0
Dmso
Aicar
Lom
Nutlin high
Nutlin low
Aicar+Lom
Aicar+Nutlin
Aicar+Torin
Lom+Nutlin
Lom+Torin
Aicar+Lom+Nutlin
Aicar+Lom+Torin
Aicar+Nutlin+Torin
Aicar+Lom+Nutlin+Torin
Treatment groups
5d (D9-D14)

E

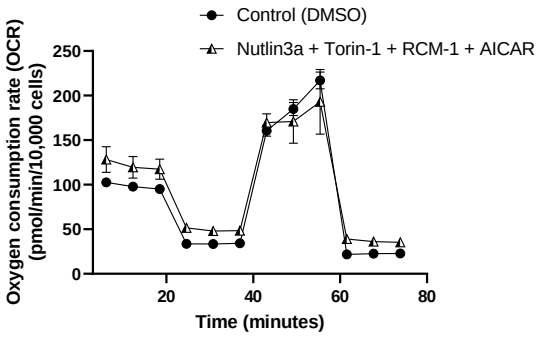
Control (DMSO)
Nutlin3a + Torin-1 + RCM-1 + AICAR
Oxygen consumption rate (OCR)
(pmol/min/10,000 cells)
250
200
150
100
50
0
20
40
60
80
Time (minutes)

F

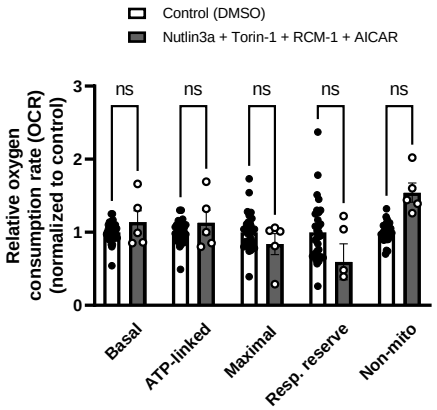
Control (DMSO)
Nutlin3a + Torin-1 + RCM-1 + AICAR
Relative oxygen
consumption rate (OCR)
(normalized to control)
3
2
1
0
ns
ns
ns
ns
ns
Basal
ATP-linked
Maximal
Resp. reserve
Non-mito

Figure S5. Extended mRNA expression and oxygen consumption rate data of combinatorial maturation treatments in iPSC-CM at day 9 of differentiation. (A) Schematic representation of the molecular and cellular effects of AICAR-induced AMPK activation taken from Sarikhani et al. [35]. (B) Relative mRNA expression of cardiac muscle genes TNNT2, (C) KCNJ2, and (D) TNNI3 by qPCR after combinatorial maturation treatment starting at day 9 of iPSC-CM differentiation, normalized to TBP and then to control DMSO treatment. (DMSO n=11 samples, all other conditions n=3 samples, plotted as mean +/- SEM). (E) Oxygen consumption rate profile and (F) oxygen consumption rate parameters after combinatorial maturation treatment starting at day 9 of differentiation, measured by Seahorse XF cell mito stress test and normalized to control DMSO treatment. ns = not significant, by one-way ANOVA with Brown-Forsythe and Welch multiple comparison analysis compared to the control treatment (DMSO n=32 wells from 2 samples, Nutlin3a + Torin-1 + RCM-1 + AICAR n=5 wells from 3 samples, plotted as mean +/- SEM). The following abbreviations and concentrations were used: control (DMSO), LOM612 (lom, 5 μM, 2 d), RCM-1 (1 μM, 5 d), Torin-1 (torin, 200 nM, 5 d), AICAR (1 mM, 5 d), Nutlin3a (nutlin/nutlin high, 10 μM, 5 d; nutlin low, 1 μM, 5 d).

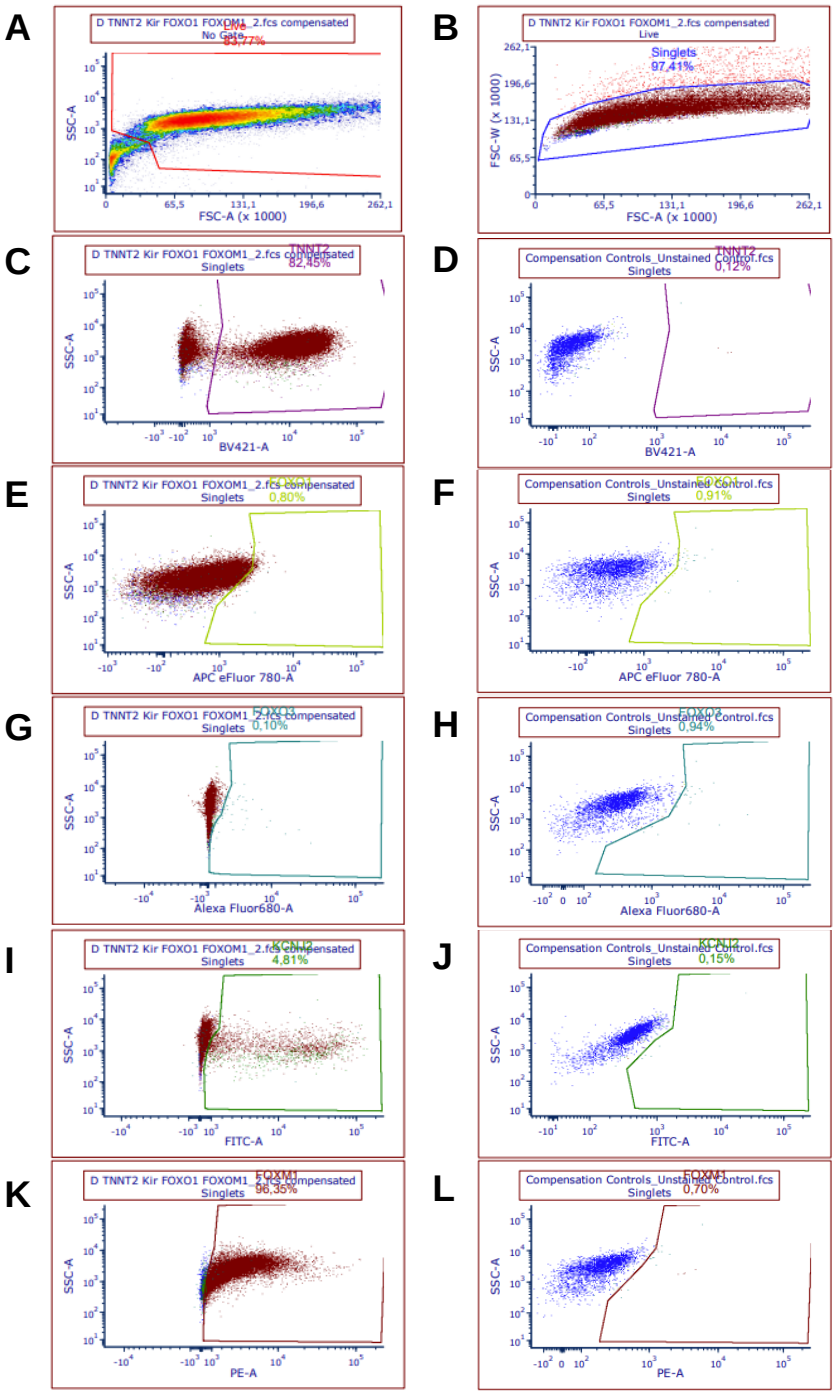

Figure S6. Flow cytometry gating for data shown in Figures 5, and S4. (A) Live cells and (B) singlet gate. (C) TNNT2-BV421 gating for a stained sample and (D) the unstained control. (E) FOXO1-AF790 gating for a stained sample and (D) the unstained control. (E) FOXO3-AF680 gating for a stained sample and (D) the unstained control. (E) KCNJ2-FITC gating for a stained sample and (D) the unstained control. (E) FOXM1-PE gating for a stained sample and (D) the unstained control.

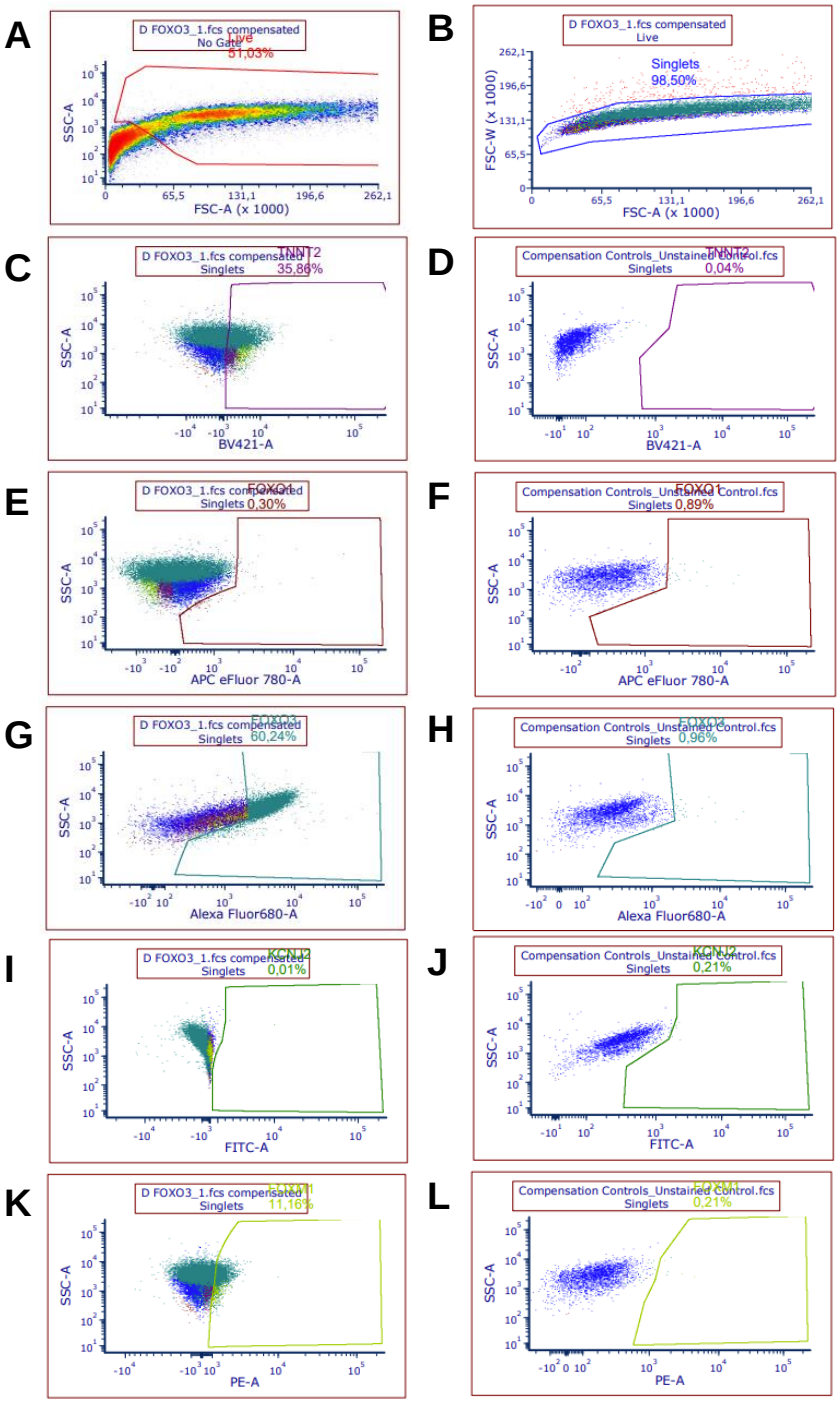

Figure S7. Flow cytometry gating for data presented in Figures 3, and S1. (A) Live cells and (B) singlet gate. (C) TNNT2-BV421 gating for a stained sample and (D) the unstained control. (E) FOXO1-AF790 gating for a stained sample and (D) the unstained control. (E) FOXO3-AF680 gating for a stained sample and (D) the unstained control. (E) KCNJ2-FITC gating for a stained sample and (D) the unstained control. (E) FOXM1-PE gating for a stained sample and (D) the unstained control.